



UNIVERSITY OF LEEDS

This is a repository copy of *Filter Or Conveyor? Establishing Relationships Between Clinoform Rollover Trajectory, Sedimentary Process Regime, and Grain Character Within Intrashelf Clinothems, Offshore New Jersey, U.S.A.*

White Rose Research Online URL for this paper:
<http://eprints.whiterose.ac.uk/130792/>

Version: Accepted Version

Article:

Cosgrove, GIE, Hodgson, DM orcid.org/0000-0003-3711-635X, Poyatos-Moré, M et al. (2 more authors) (2018) Filter Or Conveyor? Establishing Relationships Between Clinoform Rollover Trajectory, Sedimentary Process Regime, and Grain Character Within Intrashelf Clinothems, Offshore New Jersey, U.S.A. *Journal of Sedimentary Research*, 88 (8). pp. 917-941. ISSN 1527-1404

<https://doi.org/10.2110/jsr.2018.44>

© 2018 SEPM Society for Sedimentary Geology. This is an author produced version of a paper published in *Journal of Sedimentary Research*. Uploaded in accordance with the publisher's self-archiving policy. <https://doi.org/10.2110/jsr.2018.44>.

Reuse

Items deposited in White Rose Research Online are protected by copyright, with all rights reserved unless indicated otherwise. They may be downloaded and/or printed for private study, or other acts as permitted by national copyright laws. The publisher or other rights holders may allow further reproduction and re-use of the full text version. This is indicated by the licence information on the White Rose Research Online record for the item.

Takedown

If you consider content in White Rose Research Online to be in breach of UK law, please notify us by emailing eprints@whiterose.ac.uk including the URL of the record and the reason for the withdrawal request.



eprints@whiterose.ac.uk
<https://eprints.whiterose.ac.uk/>

RUNNING HEAD: CLINOFORM ROLLOVER TRAJECTORY, PROCESS-REGIME AND GRAIN-CHARACTER INTERACTIONS

TITLE: FILTER OR CONVEYOR? ESTABLISHING RELATIONSHIPS BETWEEN CLINOFORM ROLLOVER TRAJECTORY, SEDIMENTARY PROCESS-REGIME, AND GRAIN-CHARACTER WITHIN INTRASHELF CLINOTHEMS, OFFSHORE NEW JERSEY, USA

LIST OF AUTHORS: GRACE I.E. COSGROVE¹, DAVID M. HODGSON¹, MIQUEL POYATOS-MORÉ², WILLIAM D. McCAFFREY¹, NIGEL P. MOUNTNEY¹

LIST OF ADDRESSES:

¹School of Earth and Environment, University of Leeds, Leeds LS2 9JT, United Kingdom

²Department of Geosciences, University of Oslo, 0371 Oslo, Norway

CORRESPONDING AUTHOR: eeגיע@leeds.ac.uk

FIVE KEY WORDS: clinoform, trajectory, rollover, coarse-grained, process-regime

ABSTRACT

Cliniform geometries and trajectories are widely used to predict the spatial and temporal evolution of sand distribution, but most analytical approaches underplay the significance of topset/shelf process-regime in determining how and when sediment is conveyed downdip, or stored on the continental shelf. We present an integrated study of cliniform rollover trajectory and detailed grain-character analysis to assess the role of topset process-regime in determining sand distribution and sediment character across clinothems. This study targets the topset, foreset, and bottomset deposits of four successive Miocene intrashelf clinothem sequences, which represent deposition under either river-dominated or wave-dominated conditions. Seismic reflection data was combined with core analysis and grain-character data derived from 664 samples collected from 3 cored research boreholes. Within river-dominated clinothems, the transfer of coarse-grained sediment occurs under both rising and flat-to-falling cliniform rollover trajectories, suggesting that process-regime is more important in determining sediment delivery than cliniform trajectory; river-dominated systems are effective conveyors of sediment into deeper water. Wave-dominated clinothems deposited exclusively under rising cliniform rollover trajectories largely retain sand within topset and foreset deposits; wave-dominated systems are effective sediment filters. Notably, deposition under either river- or wave-dominated topset/shelf process-regimes results in quantifiable differences in grain-character attributes along cliniform profiles. Sediments in river-dominated systems are coarser, less well-rounded and more poorly sorted, and show greater inter- and intra-sequence variability than those in wave-dominated systems; prediction of sediment character is more challenging in river-dominated systems. This study highlights the need for caution when attempting to predict downdip sand distribution from cliniform trajectory alone, and provides a novel perspective into downdip grain-character profiles under end-member topset/shelf process-regime conditions. The results of this study can be used to better-constrain sediment grain-size and grain-shape distributions in process-based forward models, and have widespread applications in prediction of reservoir quality in both frontier and mature hydrocarbon basins.

INTRODUCTION

The geometry and trajectory of successive clinoform rollovers, and the resulting stacking patterns of clinothem, have been used extensively to predict the spatial location and temporal evolution of sand bodies in basin-margin successions, both in outcrop and subsurface (e.g. Steel and Olsen, 2002; Johannessen and Steel, 2005; Helland-Hansen and Hampson, 2009; Koo *et al.*, 2016; Chen *et al.*, 2018; Pellegrini *et al.*, 2017). In both clinoform trajectory models (e.g. Burgess and Hovius, 1998; Mellere *et al.*, 2002; Steel and Olsen, 2002; Bullimore *et al.*, 2005; Carvajal and Steel, 2006; Uroza and Steel, 2008; Helland-Hansen and Hampson, 2009; Ryan *et al.*, 2009) and sequence stratigraphic models (e.g. Vail *et al.*, 1977; Van Wagoner *et al.*, 1988; Van Wagoner *et al.*, 1990; Posamentier *et al.*, 1992; Johannessen and Steel, 2005; Catuneanu *et al.*, 2009), emphasis has been largely placed on the balance of accommodation and sediment supply. However, the dominant shelf process-regime also plays a key, but under-acknowledged, role in determining when coarse-grained sediment (i.e., fine sand and coarser) is stored on the continental shelf and when it is conveyed downdip (Helland-Hansen and Hampson 2009; Dixon *et al.* 2012a; Covault and Fildani 2014; Gong *et al.*, 2016; Peng *et al.*, 2017).

Recent studies have highlighted that shelf process-regime (resulting from the cumulative effects of fluvial, wave, tidal and oceanographic currents) is an important parameter to consider when predicting the presence or absence of coarse-grained sediment in downdip locations. For example, Dixon *et al.* (2012a) suggest that a river-dominated shelf-edge is critical to sand delivery into the deep-water setting. Conversely, wave- or storm-dominated shelf process-regimes are cited as ineffective conveyors of sediment to deep water, instead filtering and redistributing sediment alongshore (Plink-Björklund and Steel, 2004; Petter and Steel, 2006; Dixon *et al.*, 2012a; Gong *et al.*, 2016). However, prediction of sediment character (grain-size, grain-shape, and sorting) at different positions along the depositional profile remains poorly constrained and largely unquantified in the context of a specific

shelf process-regime. In part, this is due to the paucity of samples from coeval shelf-, slope- and basin-floor-deposits along a continuous depositional profile (Catuneanu *et al.*, 2009). To understand *how* and *when* sediments of different calibre and maturity bypass the shelf and are delivered into deep-water settings, we present new grain-character data recovered from three cores (M27, M28 and M29) that intersect shallow- and deep-marine strata from chronostratigraphically defined intrashelf clinothems, offshore New Jersey, USA. Intrashelf clinothems, also referred to subaqueous deltas, are of intermediate scale and typically have reliefs in the order of tens of meters; intrashelf clinothems are situated seaward of the shoreline break and landward of the continental break (Helland-Hansen and Hampson, 2009; Henriksen *et al.*, 2009; Helland-Hansen and Gjelberg, 2012; Patruno *et al.*, 2015; Hodgson *et al.*, 2018). The IODP Expedition 313 transect offers a rare ‘natural laboratory’ for studying the interactions of clinoform trajectory (depositional architecture) and grain-character variability due to the availability of high-resolution dip-parallel seismic data and integrated core data. High-resolution grain-character data are presented for 4 clinothem sequences, in which the clinoform trajectory has been observed from seismic reflection data, and dominant process-regimes have been interpreted from core-based observations. Three overarching research questions are addressed: 1) What are the major controls that determine clinothem architecture? 2) How does the interaction between the dominant topset/shelf process-regime and clinoform trajectory affect the timing of coarse-grained sediment delivery to deeper-water settings? 3) How do downdip grain-character profiles differ between clinothem sequences deposited under different dominant topset/shelf process-regime conditions?

The methodology and grain-character data presented here provide a unique database of grain-size, grain-shape and sorting statistics. This high-resolution grain-character database can be applied to test and refine numerical forward models (e.g. DionisosFlow, Delft2D) that seek to improve prediction of reservoir characteristics in both mature and frontier hydrocarbon basins.

Nomenclature

Hereafter, the term clinof orm is used to describe chronostratigraphic stratal surfaces, which are basinward-dipping (e.g. Gilbert, 1885; Rich, 1951; Mitchum *et al.*, 1977; Pirmez *et al.*, 1998; Patruno *et al.*, 2015). Clinof orms, at different scales, are the principal architectural element of many deltaic-to-continental slope successions (e.g. Gilbert, 1885; Rich, 1951; Mitchum *et al.*, 1977; Pirmez *et al.*, 1998).

Clinothems comprise three fundamental geometrical components: topset, foreset and bottomset deposits (Gilbert, 1885; Steel and Olsen, 2002). The foreset forms the central seaward-dipping portion of the clinothem and is the steepest part of the clinof orm sigmoid (typically dipping $\sim 1-3^\circ$ at the clinof orm inflection point). The clinof orm rollover (also referred to as the shelf-edge break, platform edge and offlap break) refers to the uppermost break in slope between the topset and foreset (Wear, 1974; Southard and Stanley, 1976; Van Wagoner *et al.*, 1990; Pirmez *et al.*, 1998; Plink-Björklund *et al.*, 2001; Glørstad-Clark *et al.*, 2010, 2011; Anell and Midtkandal, 2017 and represents a zone of increased gradient (Jones *et al.*, 2015). The base-of-slope refers to the lowermost break in clinof orm slope, between the foreset and the bottomset.

Clinof orms develop at a range of scales (e.g. Pirmez *et al.*, 1998; Steel and Olsen, 2002; Helland-Hansen and Hampson 2009; Henriksen *et al.*, 2009; Anell and Midtkandal, 2015; Patruno *et al.*, 2015), from shoreline clinof orms (1 to ~ 10 s of meters in height), to shelf-slope-basin or basin margin clinof orms (~ 100 s of meters to >1 km in height). The New Jersey intrashelf clinof orms are typically 100-300 m in height (Mountain *et al.*, 2010). This intermediate scale are referred to as intrashelf clinof orms, or subaqueous delta clinof orms, and form a component of the shelf prism. Intrashelf clinof orms are commonly located seaward of major river mouths and/or clastic shorelines but landward of the continental shelf-edge break (Hodgson *et al.*, 2018). At the shoreline delta clinof orm scale, shallow-marine and fluvial processes are dominant (e.g. wave-reworking). By contrast, at the basin-margin scale, sediment gravity flows are dominant. The New Jersey clinof orms record both physical and gravitational processes.

GEOLOGICAL SETTING

The New Jersey Atlantic margin is an example of a mid-latitude, siliciclastic-dominated, prograding passive margin, and is an ideal location to study high-resolution grain-character variability for the following reasons: i) rapid rates of deposition, which have resulted in thick accumulated sedimentary sequences (Miller and Mountain, 1994; Austin *et al.*, 1998); ii) the tectonic dormancy of the New Jersey margin, which is in the late stages of thermal cooling (Katz *et al.*, 2013); iii) good chronostratigraphic control on the timing of sedimentation (Browning *et al.* 2013); and iv) a significant volume of previously published literature that includes seismic reflection transects, outcrop and well data (Mountain *et al.*, 2010) in which the general geological setting can be framed. In 2009, the Integrated Ocean Drilling Program (IODP) Expedition 313 continuously cored and logged a nearshore portion of the New Jersey shelf margin transect (Fig. 1). The clinothems intersected during Expedition 313 and studied here are seaward-prograding, 100-300 m high intrashelf sequences of Miocene age (Mountain *et al.* 2010). The three cores (M27, M28 and M29) intersect topset, foreset and bottomset deposits (ca. 12-22Ma) along seismic line Oc270 529 (Mountain *et al.*, 2010; Kominz *et al.*, 2016) (Fig. 2).

Sequence Boundaries

The sequence boundaries of the clinothems were recognised in multichannel seismic profiles based on the location of reflector terminations (truncation, onlap, downlap and toplap) (Miller *et al.*, 2013a). The positions of sequence boundaries were confirmed through in-core identification, on the premise of physical stratigraphy and age breaks (Mountain *et al.*, 2010; Browning *et al.*, 2013; Miller *et al.*, 2013a). Miller *et al.* (2013a) concluded that they could successfully match most core and log surfaces

unequivocally with seismic sequence boundaries. The sequence stratigraphic framework presented in Miller *et al.* (2013a) provides a means of subdividing the stratigraphic record, and thus contrasting grain-character and clinothem rollover trajectory changes between individual clinothem sequences. The timings of sequence boundaries have been shown to correlate with major positive excursions in the $\delta^{18}\text{O}$ deep-sea record, suggesting that observed changes in relative sea-level (~5-20 m) are predominantly controlled by sea-level variations of allogenic origin, resulting from the waxing and waning of Antarctic ice sheets (Browning *et al.*, 2013; Kominz *et al.*, 2016).

DATA AND METHODS

Materials

The stratigraphic successions targeted during this investigation were exclusively Miocene intrashelf clinothems, correlating to depths of 225-365 mcd (meters composite depth), 312-611 mcd and 600-730 mcd in cores M27, M28 and M29, respectively. A total of 134 sediment samples were recovered from Cores 313-M27A-80-1 (224 mcd) to 313-M27A-129-2 (377 mcd) (152 m-thick sampled section). A total of 341 sediment samples were recovered from Cores 313-M28A-35-1 (311 mcd) to 313-M28A-147-1 (600 mcd) (288 m-thick sampled section). A total of 189 sediment samples were recovered from Cores 313-M29A-161-1 (600 mcd) to 313-M29A-208-1 (730 mcd) (130 m-thick sampled section). The stratigraphic interval targeted during this investigation has been subdivided into 4 depositional sequences based on the depths of the sequence stratigraphic surfaces presented in Browning *et al.* (2013): m5.7, m5.45, m5.4 and m5.3.

The Miocene clinothems are well-imaged on a grid of seismic reflection profiles (Fig. 1). Multichannel seismic profile oc270 529, shot in the region of IODP Expedition 313, transects core sites M27-M29 (Fig. 1) and provides a 2-D downdip profile of the clinothem sequences (Fig. 2). The

seismic interpretations of Monteverde *et al.* (2008), Mountain *et al.* (2010) and Browning *et al.* (2013) have been used during this investigation for correlation purposes and to subdivide the stratigraphic record into the aforementioned clinothem sequences.

Methods

Two principal methodological approaches were used in this study: high-resolution grain-character analysis and clinoform trajectory analysis. The grain-character analysis has been primarily used to produce longitudinal sediment profiles and grain-size distribution profiles, which are supplemented by core descriptions (Expedition 313 Scientists) and published seismic reflection (Monteverde *et al.*, 2008; Mountain *et al.*, 2010; Miller *et al.*, 2013a), and core sedimentology (Expedition 313 Scientists, 2010; Mountain *et al.*, 2010; Browning *et al.*, 2013; Hodgson *et al.* 2018) interpretations. The analysis of clinoform trajectory is based on the geometric properties of clinothems and through the identification of the clinoform rollover position on each seismic reflector and its evolution through time along successive intrashelf clinothem sequences (Fig. 2). Trajectory analysis was performed on high-resolution 2-D, dip-parallel seismic data. These quantitative data are supplemented by the visual core descriptions and interpretations of the Expedition 313 sedimentologists and original core observations of the sedimentary texture and structure of the core.

Grain-Character Analysis.---

The strategy for sample collection was to remove 20 cm³ sediment slices, sampled at ~0.5 m intervals down-core. In practice, there was some deviation from this sampling configuration to avoid i) horizons of cementation, ii) biscuiting disturbance (interaction of drilling fluid with sediment), iii) key stratigraphic surfaces, and iv) heavily sampled intervals.

Due to the pervasive presence of biogenic material (calcareous skeletal remains, shell fragments and organic matter) it was necessary to undertake sample pre-treatment prior to grain-character measurements, in order to remove these components. Sample pre-treatment comprised the careful manual disaggregation of samples. Rare lithified samples were disaggregated using an agate mortar and pestle (e.g. Sahu, 1964; Wilson and Pittman, 1977; Nelson, 1983; Frey and Payne, 1996; Ando *et al.*, 2014). All samples were treated with Hydrochloric Acid (10% weight to volume) (e.g. Battarbee, 1986; Battarbee *et al.*, 2001; Schumacher, 2002, Vaasma, 2008) and Hydrogen Peroxide (30% weight to volume) (e.g. Schumacher, 2002; Vaasma, 2008; Gray *et al.*, 2009), to remove calcareous and non-calcareous organic components, respectively.

Here, grain-character is defined as the grain-size, grain-shape (sphericity and roundness) and sorting of a sample. Grain-character analysis was completed using a CamsizerXT (Retsch Technology), which is an optically-based dynamic image analyser. The CamsizerXT is capable of measuring the grain-size range 1 μm – 8 mm (clay – gravel), with an accuracy of $\pm 1\%$ (Moore *et al.*, 2011). Grain-size fractions $< 1\mu\text{m}$ are lost during the process of analysis. The grain-size distributions yielded by the CamsizerXT are comparable to those produced by traditional sieving analyses. However, this instrument provides the additional advantage of simultaneous grain-shape analysis of grain sphericity and roundness. Each sample analysed by the CamsizerXT produces a dataset logarithmically divided into 105 grain-size classes, spanning 1 μm – 8 mm. The statistical analysis of all CamsizerXT results was completed using GRADISTAT computer software (Blott and Pye, 2001). The GRADISTAT software enables the rapid analysis of grain-size statistics from multiple sediment samples and produces numerical, geometrically-calculated values of the mean, mode, and sorting. Grain-shape data were analysed using Microsoft Excel software.

Clinofom Trajectory Analysis.---

The analysis of clinoform trajectory involves the identification of the clinoform rollover position on each seismic reflector analysed in this study (Fig. 2). The position of the clinoform rollover is marked by the point of maximum curvature between the topset and foreset (Pirmez *et al.*, 1998); however, delineating this position can be challenging (Olariu and Steel, 2009). To ensure consistency and repeatability, the clinoform rollover has been identified following the methodology of Anell and Midtkandal (2017, p. 282); as such, the position of the clinoform rollover is identified ‘as a point that is perpendicular to the intersection of straight lines extrapolated from the inflection point of the topset and foreset of the clinoform.’

Determination of Topset Process-Regime.---

The Expedition 313 scientists produced sedimentological interpretations of topset depositional environment using assemblages of sedimentary structures, sediment composition and texture, fossil content and ichnofabric (see Mountain *et al.*, 2010). Sedimentary facies associations presented in Mountain *et al.* (2010) indicate that the topset depositional environments of the New Jersey clinoforms varies between sequences. Relevant to this investigation, the topset deposits of Sequences m5.45 and m5.4 share features associated with wave-dominated shoreline facies models (e.g. Reineck and Singh, 1972; McCubbin, 1982; Browning *et al.*, 2006). Key diagnostic features of wave-dominated deposits (in the shoreface and shoreface-offshore transition facies) include the following: interbedded fine and very fine sands; shell debris; convex-upward laminae; low angle-angle cross-beds; symmetrical ripple lamination and moderate to heavy bioturbation (4-6 on the standard bioturbation index). Relevant to this investigation, the topset deposits of Sequences m5.7 and m5.3 share features associated with mixed river/wave delta facies models (e.g. Galloway, 1975; Bhattacharya and Walker, 1992). Key diagnostic features of river-dominated deposits include the following: coarse sands; cut-and-fill surfaces associated with basal gravels and rip-up clasts; micaceous sands; current ripple lamination and terrestrial plant material.

RESULTS

Due to the data-rich nature of this investigation, many of the data have been tabulated and/or are presented in figures. However, important differences in sedimentology (Fig. 3) and clinotherm architecture between sequences are highlighted below.

Sequence m5.7

Trajectory analysis of Sequence m5.7 indicates a slightly negative, falling trajectory (Fig. 2). At the point of core intersection, Sequence m5.7 has a thickness of 25.2 m, 44.1 m and 21.0 m in topset, foreset and bottomset locations respectively. In seismic profile, Sequence m5.7 has relatively thin topset and bottomset deposits and has relatively thicker foreset deposits (Fig. 2). The average grain-size distribution profiles of topset, foreset and bottomset deposits show very similar bimodal profiles (Fig. 4a). The finer peak is narrower and sits in the very fine sand grain-size class, and the coarser peak is broader and spans medium and coarse sand grain-size classes (Fig. 4a). The grain-size distribution profiles show progressive down-dip fining of the average grain-size composition (Fig. 3a), which corresponds to an increase in sorting (Fig. 5b) and a change in modal grain-size from medium- or coarse-grained sand in topsets to very fine or fine-grained sand in bottomset deposits (Table 1). Despite the overall down-dip fining trend, the largest (2-4 mm) and most angular grains are retained in the foreset position (Figs. 4a, 5c & d).

The up-core grain-size trends in topset and foreset deposits are dominated by ~1 m thick, very coarse-grained sand- and gravel-rich intervals (Figs. 3a & b), which typically contain ~15% very coarse-grained sand and gravel by percentage volume (Figs. 6a & b). The coarse-grained intervals are overlain by relatively fine-grained units, which are typically <1 m-thick and contain 20-25% silt by percentage volume. Topset and foreset deposits contain ~ 15% allochthonous glauconite and quartz, found within fining-upward packages and within cross-stratified sands (Table 1). The dominant up-core grain-size trend in bottomset deposits is a fining-up profile (Fig. 6c). The bottomset deposits are

relatively silt-rich (33.5%) in comparison to counterpart topset (21.5%) and foreset deposits (11%) (Fig. 6). Sedimentary structures in bottomset deposits include wavy laminations and interbedded normally graded sands and silts (mm scale), with intervals of structureless poorly sorted quartz- and glauconite-rich sands (Fig. 3c; Hodgson *et al.*, 2018). The mean grain-character profile shows a clear longitudinal profile, such that grains become increasingly rounded down-dip (Fig. 5d).

Sequence m5.45

Trajectory analysis of Sequence m5.45 indicates a positive, rising trajectory (Fig. 2). At the point of core intersection, Sequence m5.45 has a thickness of 41.1 m, 21.3 m and 11.3 m in topset, foreset and bottomset locations respectively. In seismic profile, Sequence m5.45 has relatively thick topset and foreset deposits, with relatively thin bottomset deposits (Fig. 2). The base of the foreset deposits in Sequence m5.45 has been intersected by the core. The average grain-size distribution profiles of topset, foreset and bottomset deposits are dominated by three narrow peaks in grain-size abundance at 0.068 mm (very fine-grained sand), 0.14 mm (fine-grained sand) and 0.2-0.35 mm (fine- and medium-grained sand) (Fig. 4b). The three peaks are present down-dip from topset to foreset locations with little change along the distribution profile (Fig. 4b). The longitudinal depositional profile is consistently dominated by very fine- and fine-grained sand (Figs. 3d, e & f), which is characterized by grains that are highly spherical and well-rounded (Fig. 7a & d).

Up-core grain-size trends in topset deposits indicate the development of fining-upwards packages, typically ~2.5m thick (Fig. 8a). The sedimentary structures associated with these deposits are convex-up laminated sands, containing shell fragments (Fig. 3d). Foreset and bottomset deposits contain numerous packages, which both coarsen- or fine-upwards, each typically ~2 m in thickness (Fig. 8b & c). These packages are associated with the occurrence of glauconite-rich sands above erosion surfaces, with some normal grading, and dune-scale cross-stratification in bottomset deposits (Hodgson *et al.*, 2018). There is a greater overall percentage volume of very fine- and fine-grained sand within topset

deposits than foreset and bottomset deposits (Fig. 8). Foreset deposits contain a very small contribution of very coarse-grained sand and gravel (1% and 0.5% respectively) (Figs. 4b & 8).

Mean grain sphericity remains high throughout the depositional profile, varying by less than 0.006K from topset to bottomset deposits (Fig. 7c & Table 2). Mean grain roundness shows greater variability along the depositional profile (Fig. 7d). The most angular, least well-rounded grains are found within foreset deposits. The foreset deposits also contain the least well-sorted sediments (Fig. 7b & Table 2).

Sequence m5.4

Trajectory analysis of Sequence m5.4 indicates a positive, rising trajectory (Fig. 2). In seismic profile, Sequence m5.4 displays relatively thin topset and bottomset deposits with a relatively thick foreset clastic wedge (Fig. 2), which at the point of core intersection are 23.8 m, 149.3 m and 19.2 m in topset, foreset and bottomset locations, respectively (Fig. 2). The average grain-size distribution profile of topset and foreset deposits is dominated by three narrow peaks in grain-size at 0.068mm (very fine-grained sand), 0.14mm (fine-grained sand) and 0.2-0.35mm (fine- and medium-grained sand) (Fig. 4c). The average grain-size distribution profiles remain relatively consistent from topset to foreset locations, i.e. there is little variation in the overall grain-size distribution (Fig. 4c). This is shown by the median grain-size, which varies by <0.08mm from topset to bottomset deposits (Fig. 9a). The average grain-size distribution profile of the bottomset deposits is dominated by a large peak in very coarse silt (Fig. 4c).

Up-core grain-size trends in topset deposits are dominated by fining-upward packages, typically ~2.5 m in thickness (Fig. 10a). These packages are associated with relatively clean quartz-rich sands, convex-up laminated sands (Fig. 3g), terrestrial organic matter and shell fragments. Foreset deposits are dominated by very fine- and fine-grained sands (Figs. 3b and 10e). Up-core grain-size trends in foreset deposits reveal numerous coarsening- and fining-upward packages, each typically ~7 m in

thickness (Fig. 10b). Bottomset deposits show two silt-rich intervals (Figs. 3i & 10c), interbedded with thin glauconite-rich, cross-laminated sands (Hodgson *et al.*, 2018).

Grain-shape remains relatively similar throughout the depositional profile (Figs. 9c, d & Table 3), as sediment grains within topset, foreset and bottomset deposits are highly spherical and rounded (Figs. 9c & d). Sorting increases downdip (Fig. 9b).

Sequence m5.3

Trajectory analysis of Sequence m5.3 indicates a steep rising trajectory (Fig. 2). At the point of core intersection, Sequence m5.3 has a thickness of 13.8 m, 39.8 m and 40.9 m in topset, foreset and bottomset locations respectively. In seismic profile, Sequence m5.3 has relatively thin topset deposits and relatively thick foreset and bottomset deposits (Fig. 2). The average grain-size distribution profile of topset deposits is dominated by very coarse-grained silt and very fine-grained sand (Figs. 4d). Foreset and bottomset deposits are dominated by medium- and coarse-grained sands, (43% and 40% of the total sediment volume in foreset and bottomset deposits respectively; Fig. 11e & f). The average grain-size distribution profiles of the foreset and bottomset deposits show very similar bimodal profiles, dominated by two broad peaks, corresponding to i) very coarse silt and very fine sand grain-size classes, and ii) medium sand grain-size classes (Fig. 4d). The foreset deposits have a slightly coarser overall profile and contain more very coarse-grained sand and gravel than their bottomset counterparts (Fig. 4d). The foreset and bottomset average grain-size distribution profiles show a downdip fining trend (Figs. 4d & 11), coincident with an increase in sorting (Fig. 12b) and a decrease in mean grain-size (Fig 12a & Table 4).

Topsets show no obvious trend in up-core grain-size and are consistently silt-dominated (Figs. 3j & 11a). Foreset deposits are dominated by ~1 m thick, very coarse sand- and gravel-rich intervals (Fig. 11b), which typically contain ~15% very coarse-grained sand and gravel by percentage volume (Fig. 11e). These coarser-grained intervals are overlain by relatively fine-grained units, which are typically

<1 m thick and contain 20-25% silt by percentage volume (Fig. 11b). The sedimentary structures associated with these intervals are quartz- and glauconite-rich (Fig. 3k), normally graded or cross-stratified sand beds. Bottomset deposits show broadly similar up-core grain-size dispersal patterns to those observed in foreset deposits (Fig. 11c). However, the coarse intervals are thinner (<0.7 m) and have a finer grain-size composition relative to the coarse intervals observed in foreset deposits (<0.7 m). The coarse intervals are predominantly composed of very coarse-grained sand, with minor gravels (Figs. 3l & 10c).

The mean grain-character profile varies longitudinally between parameters. Grains are decreasingly spherical downdip (Fig. 12c & Table 4). However, grain roundness shows that the most angular grains are retained in the foreset deposits, as there is an increase in roundness from the foreset to bottomset deposits (Fig. 12d & Table 4).

Clinothem Groupings

The four clinothem sequences (m5.3, m5.4, m5.45 and m5.7) have been separated into two types according to shared geometry in reflection seismic, grain-character and sedimentology.

Type A Clinothem Sequences.---

Sequences m5.7 and m5.3 constitute Type A clinothems. Core descriptions show that Type A clinothems display the following attributes: i) a lack of any convex-upward laminae (hummocky cross-stratification), low-angle cross-beds (swaley cross-stratification) or symmetrical ripple lamination; ii) cut-and-fill structures overlain by coarse sand and associated with basal gravels (e.g. Sequence m5.3, Core M27; Fig. 6a); iii) micaceous sands (e.g. Sequence m5.7, Core M27; Fig. 3j); iv) terrestrially derived plant material (e.g. Sequence m5.7, Core M27; Fig. 3j); v) foreset channel-fills

(e.g. Sequence m5.3, Core M28, 340-344 mcd; Fig. 11b) and v) bottomset deposits dominated by coarse-grained turbidites and debrites (Mountain *et al.*, 2010; Miller *et al.*, 2013a; Hodgson *et al.*, 2018). The core expression of Type A clinothems shows clear diagnostic characteristics consistent with deposition under a river-dominated topset process-regime; this interpretation is in agreement with that of Mountain *et al.*, (2010). Representative core photos are shown in Figure 3.

Sequences m5.7 and m5.3 share similar seismic and core expressions, and grain-characters, despite contrasting position in clinoform rollover trajectories (i.e. Sequence m5.7 under a falling trajectory and Sequence m5.3 under a rising trajectory; Fig. 2). Type A clinothem sequences have a seismic architecture dominated by relatively thin (14-25 m) topset deposits and thickening downdip of foreset (40-44 m) and bottomset deposits (21-41 m) (Figs. 2, 4 & 11).

Type A clinothem sequences share these common attributes: i) average grain-size distributions that fine downdip (Figs. 4a & b); ii) characteristic bimodal foreset and bottomset grain-size distribution plots (Fig. 13b); iii) the greatest volume of sand-grade sediment stored within foreset deposits (Figs. 6 & 11); iv) foreset deposits dominated by ~1m-thick very coarse sand and gravel packages overlain by relatively silt-rich packages (Figs. 6 & 11); v) the coarsest (>1.5mm) and most angular grains stored within foreset deposits (Figs. 5a, d & 12a, d); vi) an increase in sorting downdip (Figs. 5b, 12b & Tables 1, 4); and vii) glauconite- and quartz-rich structureless sands within bottomsets (Figs. 3c & l).

Type B Clinothem Sequences.---

Sequences m5.45 and m5.4 constitute Type B clinothems. Core descriptions show that Type B clinothems display the following attributes: i) widespread convex upward laminae (hummocky cross-stratification, e.g. Sequence m5.45, Core M27; Fig. 3), low-angle cross-beds (swaley cross-stratification) and symmetrical ripple lamination; ii) interbedded fine and very fine-grained sands (e.g. Sequence m5.4, Core M28; Fig. 3h); iii) significant amounts of shell debris; iv) moderate to heavy bioturbation; and v) a lack of substantial foreset or bottomset deposits indicative of gravity-flow

origin (Mountain *et al.*, 2010; Miller *et al.*, 2013a; Miller *et al.*, 2013b; Hodgson *et al.*, 2018). The core expression of Type B clinothem shows clear diagnostic characteristics consistent with deposition under a wave-dominated topset process-regime; this interpretation is in agreement with that of Mountain *et al.*, (2010). Representative core photos are shown in Figure 3.

Sequences m5.45 and m5.4 share similar core expressions and grain-characters; additionally, both Type B clinothem show consistently rising clinoform rollover trajectories. The seismic architecture of Type B clinothem is dominated by relatively thin topset (23-42 m) and bottomset deposits (12-19 m), with significantly thicker foreset deposits (~150 m) (Figs. 2, 8 & 10).

With reference to the statistical grain-character data presented in this paper, Type B clinothem share the following attributes: i) trimodal average grain-size distribution profiles; ii) grain-size compositions that vary by less than 10% along the longitudinal profile, i.e. limited downdip change in the overall grain-size composition and distribution (Figs. 4b, c, 8 & 10); iii) limited downdip change in grain-character (Figs. 7c, d & 9c, d), including a <0.04K change in sphericity and roundness (Tables 2, 3); iv) the highest mud content within topsets (~25%) (Figs. 8 & 10) and v) coarsening- and fining-upward packages within foresets, although these are more numerous and better developed in Sequence m5.4 (Figs. 8b & 10b).

DISCUSSION

Controls on differences between Type A and B Clinothem

Clinothem Types A and B fundamentally differ in many aspects of grain-character. Differences in sediment character are controlled by the interplay of accommodation, climate, sediment supply, provenance, and dominant topset/shelf process-regime. On the ocean-facing passive margin location of New Jersey, changes in accommodation are closely tied to changes in eustatic sea level (Browning

et al., 2013). Eustasy is largely discounted as a controlling factor to explain differences between Type A and Type B clinothems because each clinothem sequence represents one complete sea-level cycle and associated regression to transgression (Miller *et al.* 2013a). As such, the effects of eustasy should be common to each sequence. However, it is acknowledged that sea-level fluctuations are not necessarily uniform in amplitude or rate, which could impact differences in clinothem development. A similar argument can be made for climate, as each clinothem sequence theoretically records one complete climatic cycle. However, this argument pertains to regional climatic regime and does not necessarily account for the effects of variability in local climate, which may influence rainfall and consequently sediment supply rates.

Rates of sediment supply have been estimated for Sequences m5.3 (Type A), and Sequences m5.4 and m5.45 (Type B), using integrated strontium isotope stratigraphy and biostratigraphy age-depth plots (Browning *et al.*, 2013). However, there are not sufficient data available for Sequence m5.7 (Type A) due to poor age constraints. Comparisons between sediment supply rates of sequences were made by averaging sedimentation rates across clinothems. Results indicate that within the bottomset deposits of Sequences m5.4 and m5.45 (Type B), minimum rates of deposition were 96 m/Myr. Similarly, Sequence m5.3 (Type A) had a minimum rate of 100 m/Myr. Topsets deposits indicate that Sequences m5.45, m5.4 and m5.3 (Type A and B) had the same minimum rates of deposition of 43 m/Myr. This suggests that rates of sediment supply did not differ significantly during deposition of clinothem Types A and B in topset and bottomset locations, and therefore that sediment supply rates did not cause the observed differences in grain-character between Type A and Type B clinothems. The lack of variability in sediment supply rates also supports the assertion that accommodation and climate did not differentially impact Type A and B clinothems significantly. However, it must be acknowledged that there are significant age-control error margins and there is a lack of data for Sequence m5.7 (Type A) and also that the comparison does not take into account along-strike variability.

Accepting that the Type A and B clinothems appear to have developed under comparable allogenic forcings (i.e. with respect to accommodation and sediment supply) and prograded during the Burdigalian (Browning *et al.*, 2013), a period of time without a recognised large-scale climatic

perturbation, the remaining forcing mechanism to consider is that of the dominant process-regime. The expression in core of the four clinothems studied in this investigation permits confident distinction of the dominant process-regime during the development of both Type A and Type B clinothems, which were river- and wave-dominated, respectively (Fig. 3). It is therefore suggested that the difference in the dominant topset process-regime had significant bearing on the differences in sediment character and depositional character observed between and within Type A and Type B clinothems.

Lateral Variability in Process-Regime

The dataset presented and discussed, which comprises a 2-D dip-parallel transect of seismic reflection data and three cores that intersect the topset, foreset and bottomset deposits of prograding clinothems, has both strengths and weaknesses. The New Jersey clinothems are rare examples where the sedimentological and stratigraphic characteristics of coeval topset, foreset and bottomset deposits have been documented in successive chronostratigraphically constrained clinothems. No previous dataset of such detailed quantitative grain-character analysis on genetically-linked clinothems has been presented.

There is a network of 2D seismic reflection lines that allow the 3D architecture of the clinothems to be constrained (Monteverde et al. 2008). However, the core dataset is from a single 2-D transect. Modern and ancient shallow-marine systems can exhibit high levels of lateral variability, even over relatively short distances of a few hundreds of meters, related to the relative importance of fluvial, wave and tidal processes (Ta et al., 2002; Bhattacharya and Giosan, 2003; Ainsworth *et al.*, 2008; 2011; Vakarelov and Ainsworth, 2013; Olariu, 2014; Jones *et al.* 2015). Lateral changes in the process regime could impact the timing of sand delivery into the deeper basin (Madof *et al.*, 2016), the location of coarse-grained deposits (Carvajal and Steel 2009; Koo *et al.*, 2016) and the spatial distribution of grain-character of the foresets and bottomsets. For example, a wave-dominated system might transition laterally to a river-dominated system in the topsets, but downdip of the wave-

dominated system a fan fed by the river-dominated system could be intersected. Nonetheless, the dataset present here has permitted for the first time high-resolution quantitative assessment of grain-character to be discussed in relation to clinoform trajectory and topset process-regime. Future investigations into the interplay of lateral variability in process-regime and distribution of grain character will require exceptional exhumed systems with 3D control, or integrated subsurface datasets of 3D reflection seismic data and additional research core holes.

Interaction of Shelf Process-Regime and Clinoform Rollover Trajectory

Type A Clinothem Sequences.---

Based on core-observations, the Type A clinothems (Sequence m5.7 and m5.3) are interpreted to be river-dominated, although lateral variability in process-regime as a control on sediment distribution to the foreset and bottomsets cannot be discounted (e.g. Ainsworth *et al.*, 2011; Olariu, 2014; Jones *et al.* 2015; Rossi and Steel, 2016). Type A clinothems (river-dominated; Fig. 14a) show variability in their clinoform rollover trajectories, such that Sequence m5.7 has a rising trajectory and Sequence m5.3 has a falling trajectory (Fig. 2). However, both of the documented Type A clinothems have foreset and bottomset deposits that contain substantial quantities of coarse-grained sediment (Figs. 4 & 11). This indicates that the downdip transport of coarse-grained sediment can occur under both falling and rising clinoform rollover trajectories, within Type A clinothem sequences. This finding would not be predicted by applying conventional sequence stratigraphic models and clinoform trajectory analyses (e.g. Steel and Olsen, 2002; Johannessen and Steel, 2005; Helland-Hansen and Hampson, 2009). In fact, the grain-size data presented here show a greater overall proportion of coarse-grained sediment in Sequence m5.3 (rising trajectory) relative to Sequence m5.7 (falling trajectory). The occurrence of coarse-grained sediment in foreset and bottomset deposits implies that a river-dominated process-regime at the clinoform rollover may be a more important factor in determining coarse-grained sediment delivery than clinoform trajectory alone, in agreement with Dixon *et al.* (2012a).

In addition to having different clinoform rollover trajectories, the topset deposits of Sequences m5.7 and m5.3 also differ in grain-size composition. Sequence m5.7 has a silt-rich base (355-361 mcd), which progressively coarsens upwards, to contain ~20% very coarse sand and gravel by percentage volume (336-355 mcd) (Fig. 4a). By contrast, the topset deposits of Sequence m5.3 are dominated by silt-prone sediments and lack the coarse-grained sediment components observed in Sequence m5.7 (Fig. 11a). The variable nature of the topset deposits of Type A clinothem sequences may reflect along-strike variability in depositional environments of river-dominated process-regimes (Fig. 14a); examples of such lateral variability in shelf systems is documented in both modern and ancient delta systems (e.g. Ta *et al.*, 2002; Gani and Bhattacharya, 2007; Carvajal and Steel 2009; Olariu, 2014; Li *et al.*, 2015). Alternatively, or in addition to this, the inter-sequence topset grain-size variability may reflect erosive conditions landward of the clinoform rollover, such that the upper topset deposits of Sequence m5.3 may have been eroded during regression or transgression, removing the coarser sediment fractions.

Erosive conditions landward of the clinoform rollover during regression is supported by the presence of significant volumes of allochthonous glauconite within the foreset and bottomset deposits of both Type A clinothem sequences (Hodgson *et al.*, 2018), which can form up to 90% of the total sediment volume (Tables 1 & 4). The presence of reworked glauconite (likely to be originally formed in transgressive shoreface sands in topset environments) in downdip environments is suggestive of erosive conditions in the topset, such that shallow-water glauconite grains are entrained and transported into deeper-water settings. The glauconite-bearing mud-prone sands, which are poorly sorted and poorly stratified, are interpreted to be debrites (debris-flow deposits; Mulder and Alexander, 2001) intercalated with thin turbidites (Hodgson *et al.*, 2018). A predominantly debritic flow-regime is further evidenced by the presence of pristine benthic foraminifera and thin-walled articulated shells scattered in the glauconite-bearing mud-prone sands, suggesting a cohesive flow with minimal internal turbulence (see Hodgson *et al.*, 2018). Similar sediment transport processes for Type A clinothem sequences beyond the clinothem rollover is supported by the similar grain-size

distributions (Figs. 13b & c), grain-size patterns (Figs. 4 & 11) and core lithologies observed within the foreset and bottomset deposits of Type A clinothem sequences (Fig. 3).

Despite evidence for debris flow and turbidity current processes in operation within the Type A clinothem sequences, seismic and core data do not support the presence of any major incisional features on the clinoform rollover (Hodgson *et al.*, 2018). This somewhat disagrees with conventional models, which are based on the argument that river-dominated systems have the ability to rapidly prograde across the shelf and form large fluvial networks that incise the clinoform rollover and transfer significant volumes of coarse-grained sediment into bottomset deposits (e.g. Vail *et al.*, 1997; Van Wagoner *et al.*, 1988; 1990; Posamentier *et al.*, 1992; Johannessen and Steel, 2005; Carvajal and Steel, 2006; Catuneanu *et al.*, 2009, Sanchez *et al.*, 2012). In this instance, the lack of any observable large incisional features on the clinoform rollover (Fig. 2) instead suggests the presence of a network of smaller sediment distributary channels (Hodgson *et al.*, 2018).

The fluvial distributary channel network, supplying sediment to bottomset deposits, was likely to be active during periods of high sediment discharge (*sensu* Carvajal and Steel, 2006), and might have been associated with river flooding, storms, or combined events. However, the lack of evidence of subaerial exposure of the clinoform rollover (Mountain *et al.*, 2010), suggests that river-systems may not have transferred sediment directly into foreset and bottomset deposits. Instead river flooding, storm, or combined events may have triggered clinoform-rollover sediment failure, remobilising glauconite- and quartz-rich sediment temporarily stored within topset deposits (*sensu* Chen *et al.*, 2018). This mixed supply system may account for the consistent bimodal nature of Type A foreset and bottomset deposits (Fig. 13b &c), insofar as the very coarse-grained silt and very fine-grained sand component may reflect direct suspended riverine sediment discharge and the medium- and coarse-grained sand may reflect transient deposition of clinoform-rollover sands.

The bimodality of grain-size in Type A clinothems highlights a paucity of grain-size fractions spanning very fine to fine sand (0.088-0.18 mm) (Fig. 13b & c). This may reflect a scarcity of these grain-size classes within the hinterland source area, i.e. these grain-size classes are not delivered to the continental shelf. Alternatively, the absence of these grain sizes may reflect selective sediment

bypass, such that these grain-size fractions were preferentially bypassed into deeper-water than that sampled by Core M29 (*sensu* Stevenson *et al.*, 2015).

This study indicates that, although coarse-grained sediment delivery can take place in river-dominated conditions under both rising- and falling-trajectories, fluvial entrenchment of the clinoform rollover is not required (e.g. Ryan *et al.*, 2009; Dixon *et al.*, 2012a). However, the lack of clinoform rollover incision may affect sediment distribution within the system. This is expressed in the longitudinal grain-character profile, insofar as smaller distributary networks do not have the necessary energy to transport the coarsest-sediment fractions into bottomset deposits. This results in the largest, most angular grains being deposited within foresets (Fig. 14c & f).

Type B Clinothem Sequences.---

Type B clinothems (Sequences m5.45 and m5.4) consistently have rising clinoform rollover trajectories (Fig. 2) and are characterised by wave-dominated process-regimes (Mountain *et al.*, 2010; Fig. 14b). We observe relatively thin (<20 m in thickness) bottomset deposits (Fig. 2), which contain no gravel and <0.5% coarse sand by percentage volume. This is interpreted to indicate limited bypass of coarse-grained sediments into bottomset deposits (Figs. 8 & 10). The absence of coarse-grained sediment in bottomset deposits also reflects the lack of coarse-grained sediment fractions throughout the Type B depositional profile as whole (Figs. 8 & 10). This suggests that, under wave-dominated conditions, the coarser sediment fractions are redistributed by shore-parallel processes, spreading coarse-grained sand over the nearshore margin. Thus, open-sea conditions under wave-dominated processes inhibit the transport of coarse-grained sediment to the clinoform rollover, reducing the potential for downdip sediment transport. These observations conform to conventional sequence stratigraphic and rollover-trajectory model that predict limited bypass of coarse-grained sediment downdip under these circumstances, with preferential retention of sediment within shelf-environments (Steel and Olsen, 2002; Deibert *et al.*, 2003; Johannessen and Steel, 2005; Carvajal and Steel, 2009),

and the development of shore-parallel sand bodies (e.g. Davis and Hayes, 1984; Bhattacharya and Giosan, 2003). Consequently such regimes have little potential to generate incisional features on the clinoform rollover, limiting downdip transfer of coarse-grained sediment (Sydow and Roberts, 1994; Johannessen and Steel, 2005; Peng *et al.*, 2017), provided that no canyon intersects the longshore drift zone (Covault *et al.*, 2007; Boyd *et al.*, 2008; Dixon *et al.*, 2012b).

The depositional profiles of Type B clinothem are dominated by very fine- and fine-grained sands, which are highly spherical and rounded relative to Type A river-dominated clinothem (Fig. 14e & f). This likely reflects wave reworking and longshore drift processes in the topsets of wave-dominated clinothem, which produce relatively clean shoreface sands (e.g. Roy *et al.*, 1994; Bowman and Johnson, 2015). Grain-rounding by additional wave resuspension processes produces a more uniform sediment grain-size distribution in Type B clinothem (Fig. 14c), which lack the fine and coarse grain-size outliers observed within Type A river-dominated clinothem (Fig. 13).

Type B clinothem exhibit intragroup variability, such that the foreset and bottomset deposits of Sequence m5.45 and m5.4 differ subtly (Figs. 8 & 10). Sequence m5.45 has foreset and bottomset deposits that contain thin packages of coarse-grained sediments (e.g. Core M28, 523-528 mcd), associated with reworked glauconite (Fig. 8). These coarse-grained packages are absent in Sequence m5.4 (Fig. 10). The glauconitic, coarser packages account for higher mean grain-size observed within the foreset and bottomset deposits of Sequence m5.45 relative to Sequence m5.4 (Fig. 14c). In addition, the foreset deposits of Sequence m5.45 are more poorly sorted (Fig. 14d), and have less spherical (Fig. 14e) and more angular grains (Fig. 14f) relative Sequence m5.4. The glauconite-rich, coarse-grained packages are mainly associated with turbiditic sedimentary features, including normally-graded and cross-laminated glauconite-sands (Hodgson *et al.* 2018). However, the topsets of both sequences are similar, displaying comparable up-core grain-size patterns, grain-size distributions and sorting (Figs. 8, 10 & 13d). The divergence in grain-character between Sequence m5.45 and m5.4 becomes greater downdip (Figs. 14d, e & f). This implies topset-bypass of the glauconite-rich, coarse-grained sediment and/or its erosion and reworking beyond the clinoform rollover, but perhaps with larger sediment supply and coarse-grained sediment availability in Sequence m5.45. Under either of

these circumstances (i.e. topset bypass and/or erosion beyond the clinoform rollover), a highly erosional, turbidity current would be required to i) transport coarse-grained sediment across the topset, ii) bypass the high-energy coastal fence of longshore drift, and/or iii) erode and remobilise coarse-grained sediments from underlying foreset deposits. This implies one or multiple episodic returns to river-dominated process-regime conditions, suggesting that Sequence m5.45 an example of mixed wave- and river-dominated clinoform rollover conditions (e.g. Gomis-Cartesio *et al.*, 2017) (Fig. 14b).

CONCLUSIONS

High-resolution grain-character analysis, integrated with core sedimentology and clinoform rollover trajectory analysis of Miocene intrashelf clinothems, located offshore New Jersey, has allowed identification and detailed characterisation of archetypal river- and wave-dominated longitudinal sedimentary profiles of clinothems for the first time (Fig. 14). River-dominated (Type A) clinothems, which display falling, flat, and rising clinoform rollover trajectories, are associated with considerable transport of coarse-grained sediment downdip. These conditions are associated with the following: i) inconsistent topset deposits, reflecting erosive conditions landward of the clinoform rollover; ii) coarse-grained sediment delivery into foreset and bottomset deposits, via both turbiditic and debritic flow regimes, potentially triggered by river-flooding- or storm-remobilisation of glauconite-rich sands at the clinoform rollover; and iii) deposition of the coarsest, least spherical and most angular grains within foreset deposits, resulting from the rapid dissipation of energy, associated with multiple feeder channels and no major incision of the clinoform rollover. The largest volumes of coarse-grained sediment are delivered into downdip settings from fluvial-dominated topsets.

Wave-dominated (Type B) clinothem sequences generally conform to traditional models, such that Sequences m5.45 and m5.4 both have rising trajectories, relatively thin bottomset deposits and minimal coarse-grained sediment throughout their depositional profiles. Wave-dominated conditions

are associated with the following: i) longitudinal sediment profiles dominated by rounded, highly spherical very fine- and fine-grained sands, associated with wave reworking landward of the clinoform rollover; ii) minimal occurrence of coarse-grained sediment throughout the depositional profile, possibly associated with shore-parallel coarse-grained sediment redistribution; and iii) a grain-size distribution with limited downdip variation, associated with wave-resuspension grain-size sorting. Sequence m5.45 also shows non end-member characteristics, including glauconite-rich, turbiditic sands, and represents a locally mixed wave-dominated and river-influenced process-regime.

Through analysis of multiple clinothems the integrated dataset reveals a breakdown in the predicted relationship between clinoform trajectory and the delivery of coarse-grained sediment into deep-water settings. Process-regime in the topset/shelf is a key factor controlling basinward transfer of coarse-grained sediment, which can be bypassed into bottomset deposits in river-dominated clinothems under both rising and falling clinoform rollover trajectories. As such, clinoform trajectory alone is not a reliable predictor of the presence of coarse-grained sediment in the absence of a good facies and grain-size distribution control. Identification of the dominant process-regime alongside clinoform trajectory analysis is a more effective approach in determining the presence or absence of coarse-grained sediment deposits. The integrated high-resolution grain-character and clinoform trajectory analysis presented in this paper highlights the need for ongoing critical evaluation of conventional sequence stratigraphic and clinoform trajectory paradigms.

This study clearly demonstrates that the physical processes in action on the shelf, i.e. the interaction between fluvial- and wave-processes, exert a fundamental control on grain-character distributions, and therefore reservoir quality. Furthermore, not only do fluvial- and wave-processes impact the grain-size, grain-shape and sorting of shelf deposits, they change the reservoir characteristics across the complete depositional profile from topset (shelf) to foreset (slope) to bottomset (basin-floor). This new quantitative dataset will have widespread use and value for improving numerical models, which seek to accurately replicate the sediment-export properties of depositional systems under specific shelf process-regime conditions.

ACKNOWLEDGMENTS

We thank the Integrated Ocean Drilling Program (IODP), ECORD Science Operator (EOS) and the Bremen Core Repository (BCR) for assisting us with the process of sample collection. We thank the Sorby Environmental Fluid Dynamics Laboratory (University of Leeds) for assistance with sample analysis. Finally, we thank reviewers C. Olariu, C. Robin, Associate Editor A. Fildani and Editor G. Hampson for their constructive comments that significantly improved the paper.

REFERENCES

- Ainsworth, R. B., Flint, S.S., Howell, J.A., 2008, Predicting coastal depositional style: Influence of basin morphology and accommodation to sediment supply ratio within a sequence-stratigraphic framework, *in*: Hampson, G.J., Steel, R.J., Burgess, P.M., Dalrymple, R.W., eds., Recent advances in models of shallow-marine stratigraphy: SEPM Special Publication, v. 90, p. 237-263
- Ainsworth, R.B., Vakarelov, B.K., Nanson, R.A., 2011, Dynamic spatial and temporal prediction of changes in depositional processes on clastic shorelines: toward improved subsurface uncertainty reduction and management: American Association of Petroleum Geologists, Bulletin, v. 95, p. 267-297
- Ando, H., Oyama, M., Nanayama, F., 2014, Data report: grain size distribution of Miocene successions IODP Expedition 313 Sites M0027, M0028 and M0029, New Jersey shallow shelf, *in* Mountain, G., Proust, J.-N., McInroy, D., Cotterill, C., and the Expedition 313 Scientists, Proceedings of the Integrated Ocean Drilling Program, Vol. 313
- Anell, I., Midtkandal, I., 2017, The quantifiable clinotherm- types, shapes and geometric relationships in the Plio-Pleistocene Giant Foresets Formation, Taranaki Basin, New Zealand: Basin Research, v. 29, p. 277-297

- Austin, J.A., and 27 others, 1998, Initial reports of the Ocean Drilling Program, Leg 174A: College Station, Texas, Ocean Drilling Program, p. 324
- Battarbee, R. W., 1986, Diatom analysis, *in* Berglund, B. E., ed., Handbook of Holocene Palaeoecology and Palaeohydrology, John Wiley & Sons, Toronto, p. 527-570.
- Battarbee, R. W., Jones, V. J., Flower, R. J., Cameron, N. G., Bennion, H. 2001, Diatoms, *in* Smol, J. P., Birks, H. J. B. & Last, W. M., eds., Tracking Environmental Change Using Lake Sediments, Volume 3: Terrestrial, Algal and Siliceous Indicators, Kluwer Academic Publishers, Dordrecht, v. 3, p. 155-202
- Bhattacharya, J.P., Giosan, L., 2003, Wave-influenced deltas: geomorphological implications for facies reconstruction: *Sedimentology*, v. 50, p. 187-210.
- Bhattacharya, J.P., Walker, R.G., 1992, Deltas, *in* Walker, R.G., James, N.P., eds., Facies Models: Response to Sea Level Change: St. John's, Newfoundland: Geological Association of Canada, p. 157-177
- Blott, S.J., Pye, K., 2001, GRADISTAT: a grain size distribution and statistics package for the analysis of unconsolidated sediments: *Earth Surface Processes and Landforms*, v. 26, p. 1237-1248
- Bowman, A. P., Johnson, H. D., 2014, Storm-dominated shelf-edge delta successions in a high accommodation setting: The palaeo-Orinoco Delta (Mayaro Formation), Columbus Basin, South-East Trinidad: *Sedimentology*, v. 61, p. 792-835
- Boyd, R., Ruming, K., Goodwin, I., Sandstrom, M., Schröder-Adams, C., 2008, Highstand transport of coastal sand to the deep ocean: a case study from Fraser Island: *Southeast Australia Geology*, v. 36, p. 15-18
- Browning, J.V., Miller, K.G., McLaughlin, P.P., Kominz, M.A., Sugarman, P.J., Monteverde, D., Feigenson, M.D., Hernández, J.C., 2006, Quantification of the effects of eustasy, subsidence, and

sediment supply on Miocene sequences, mid-Atlantic margin of the United States: Geological Society of America Bulletin, v. 118, p. 567-588

Browning, J.V., Miller, K.G., Sugarman, P.J., Barron, J., McCarthy, F.M.G., Kulhanek, D.K., Katz, M.E., Feigenson, M.D., 2013, Chronology of Eocene-Miocene sequences on the New Jersey shallow shelf: Implications for regional, interregional, and global correlations: Geosphere, v. 9, p. 1434-1456

Bullimore, S., Henriksen, S., Liestøl, F.M., Helland-Hansen, W., 2005, Clinofolds stacking patterns, shelf-edge trajectories and facies associations in tertiary coastal deltas, offshore Norway: implications for the prediction of lithology in prograding systems: Norwegian Journal of Geology, v. 85, p. 167-187

Burgess, P.M., Hovius, N., 1998, Rates of delta progradation during highstands: consequences for timing of deposition in deep-marine systems: Geological Society of London, Journal, v. 155, p. 217-222

Carvajal, C., Steel, R., 2006, Thick turbidite successions from supply-dominated shelves during sea-level highstand: Geology, v. 34, p. 665-668

Carvajal, C., Steel, R., 2009, Shelf-edge architecture and bypass of sand to deep water: influence of shelf-edge processes, sea level and sediment supply: Journal of Sedimentary Research, v.79, p.652-672

Catuneanu, O., Abreu, V., Bhattacharya, J.P., Blum, M.D., Dalrymple, R.W., Eriksson, P.G., Fielding, C.R., Fisher, W.L., Galloway, W.E., Gibling, M.R., Giles, K.A., Holbrook, K.A., Jordon, J.M., Kendall, R., Macurda, C.G. St., Macurda, C.B., Martinsen, O.J., Miall, A.D., Neal, J.E., Nummedal, D., Pomar, L., Posamentier, H.W., Pratt, B.R., Sarg, J.F., Shanley, K.W., Steel, R.J., Strasser, A., Tucker, M.E.C., 2009, Towards the standardization of sequence stratigraphy: Earth Science Reviews, v. 92, p. 1-33

Chen, S., Steel, R., Olariu, C., Li, S., 2018, Growth of the paleo-Orinoco shelf margin prism: Process regimes, delta evolution, and sediment budget beyond the shelf edge: *The Geological Society of America Bulletin*, v. 130, p. 35-63

Covault, J.A., Normark, W.R., Romans, B.W., Graham, S.A., 2007, Highstand fans in the California borderland: the overlooked deepwater depositional systems: *Geology*, v. 35, p. 783-786

Covault, J.A. and Fildani, A., 2014, Continental shelves as sediment capacitors or conveyors: source-to-sink insights from the tectonically active Oceanside shelf, southern California, USA, *in* Chiocci, F.L., Chivas, A.R., eds., *Continental Shelves of the World: Geological Society, London, Memoirs*, v. 41, p. 315-326

Davis, Jr., R.A., Hayes, M.O., 1984, What is a Wave-Dominated Coast?: *Marine Geology*, v. 60, p. 313-329

Deibert, J.E., Benda, T., Løseth, T., Schellpeper, M., Steel, R.J., 2003, Eocene Clinoform Growth in Front of a Storm-Wave-Dominated Shelf, Central Basin, Spitsbergen: No Significant Sand Delivery to Deepwater Area: *Journal of Sedimentary Research*, v. 23, p. 546-558

Dixon, J.F., Steel, R.J., Olariu, C., 2012a, Shelf-edge delta regime as a predictor of the deep-water deposition: *Journal of Sedimentary Research*, v. 82, p. 681-687

Dixon, J.F., Steel, R.J., Olariu, C., 2012b, River-dominated shelf-edge deltas: delivery of sand across the shelf break in the absence of slope incision: *Sedimentology*, v. 59, p. 1133-1157

Expedition 313 Scientists, 2010, Site M0028, *in* Mountain, G.S., Proust, J-N., McInroy, D., Cotteril, C., and the Expedition 313 Scientists, 2010, *Proceedings of the Integrated Ocean Drilling Program, Expedition 313: Tokyo, Integrated Ocean Drilling Program Management, Inc.*

Folk, R.L., Ward, W.C., 1957, Brazos River bar: a study in the significance of grain size parameters: *Journal of Sedimentary Petrology*, v. 27, p. 3-26

Frey, M.H., Payne, D.A., 1996, Grain-Size effect on Structure and Phase Transformations for Barium Titanate: *Physical Review*, v. 54, p. 3158-3168

Galloway, W.E., 1975, Process framework for describing the morphologic and stratigraphic evolution of deltaic depositional systems, *in* Broussard, M.L., ed., *Deltas: Models for Exploration*: Houston Geological Society, p. 87-98

Gani, M.R., Bhattacharya, J.P., 2007, Basic building blocks and process variability of a Cretaceous delta: internal facies architecture reveals a more dynamic interaction of river, wave, and tidal processes than is indicated by external shape: *Journal of Sedimentary Research*, v. 77, p. 284-302

Gilbert, G.K., 1885, The topographic feature of lake shores: U.S. Geological Survey, Annual Report, v. 5, p. 104-108

Glørstad-Clark, E., Birkeland, E.P., Nystuen, J.P., Faleide, J.I., Midtkandal, I., 2011, Triassic platform-margin deltas in the Western Barents Sea: *Marine and Petroleum Geology*, v. 28, p. 1294-1314

Glørstad-Clark, E., Faleide, J.I., Lundschie, B.A., Nystuen, J.P., 2010, Triassic seismic sequence stratigraphy and paleogeography of the Western Barents Sea area: *Marine and Petroleum Geology*, v. 27, p. 1448-1475

Gomis-Cartesio, L.E., Poyatos-Moré, M., Flint, S.S., Hodgson, D.M., Brunt, R.L., Wickens, H.D.V., 2017, Anatomy of a mixed-influence shelf edge delta, Karoo Basin, South Africa, *in*: Hampson, G.J., Reynolds, A.D., Kostic, B., Wells, M.R., eds., *Sedimentology of Paralic Reservoirs: Recent Advances*: Geological Society Special Publications, v. 444, p. 393-418

Gong, C., Steel, R.J., Wang, Y., Lin, C., Olariu, C., 2016, Grain size and transport regime at shelf edge as fundamental controls on delivery of shelf-edge sands to deepwater: *Earth-Science Reviews*, v. 157, p. 32-60

Gray, A.B., Pasternack, G.B., Watson, E.B., 2009, Hydrogen peroxide treatment effects on the particle size distribution of alluvial and marsh sediments: *The Holocene*, v. 20, p. 293-301

Helland-Hansen, W., Gjelberg, H., 2012, Towards a hierarchical classification of clinoforms: AAPG Annual Convention and Exhibition, April 22–25, 2012, Long Beach, California, U.S., Search and Discovery article #90142

Helland-Hansen, W., Hampson, G.J., 2009, Trajectory analysis: concepts and applications: *Basin Research*, v. 21, p. 454-483

Henriksen, S., Hampson, G.J., Helland-Hansen, W., Johannessen, E.P., Steel, R.J., 2009, Shelf edge and shoreline trajectories, a dynamic approach to stratigraphic analysis: *Basin Research*, v. 21, p. 445-453

Hodgson, D.M., Browning, J.V., Miller, K.G., Hesselbo, S., Poyatos-Moré, Mountain, G.S., Proust, J.-N., 2018, Sedimentology, stratigraphic context, and implications of Miocene bottomset deposits, offshore New Jersey, 2017: *Geosphere*, v. 14, p. 95-114

Johannessen, E.P., Steel, R.J., 2005, Shelf-margin clinoforms and prediction of deepwater sands: *Basin Research*, v. 17, p. 521-550

Jones, G.E.D., Hodgson, D.M., Flint, S.S., 2015, Lateral variability in clinoform trajectory, process regime, and sediment dispersal patterns beyond the shelf-edge rollover in exhumed basin margin-scale clinothem: *Basin Research*, v. 27, p. 657-680

Katz, M.E., Browning, J.V., Miller, K.G., Monteverde, D.H., Mountain, G.S., Williams, R.H., 2013, Paleobathymetry and sequence stratigraphic interpretations from benthic foraminifera: Insights on New Jersey shelf architecture, IODP Expedition 313: *Geosphere*, v. 9, p. 1488-1513

Kominz, M.A., Miller, K.G., Browning, J.V., Katz, M.E., Mountain, G.S., 2016, Miocene relative sea level on the New Jersey shallow continental shelf and coastal plain derived from one-dimensional backstripping: A case for both eustasy and epeirogeny: *Geosphere*, v. 12, p. 1437-1456

Koo, W.M., Olariu, C., Steel, R.J., Olariu, M.I., Carvajal, C.R., Kim, W., 2016, Coupling between shelf-edge architecture and submarine fan growth style in a supply-dominated margin: *Journal of Sedimentary Research*, v. 88, p. 613-628

Krumbein, W.C., 1941, Measurement and geological significance of shape and roundness of sedimentary particles: *Journal of Sedimentary Petrology*, v. 11, p. 64-72

Li, Z., Bhattacharya, J., Schieber, J., 2015, Evaluating along-strike variation using thin-bedded facies analysis, Upper Cretaceous Ferron Notom Delta, Utah: *Sedimentology*, v. 62, p. 2060-2089

Madof, A.S., Harris, A.D., Connell, S.D., 2016, Nearshore along-strike variability: Is the concept of the systems tract unhinged?: *Geology*, v. 44, p. 315-318.

McCubbin, D.G., 1982, Barrier-island and strand-plain facies, *in* Scholle, P.A., and Spearing, D., eds., *Sandstone Depositional Environments: American Association of Petroleum Geologists Memoir*, v. 31 p. 247-279

Mellere, D., Plink-Björklund, P., Steel, R., 2002, Anatomy of shelf deltas at the edge of a prograding Eocene shelf margin, Spitsbergen: *Sedimentology*, v. 49, p. 1181-1206

Miller, K.G., and Mountain, G.S., 1994, Global sea-level change and the New Jersey margin, *in* Mountain, G.S., et al., eds., *Proceedings of the Ocean Drilling Program, Initial Reports, Volume 150*: College Station, Texas, Ocean Drilling Program, p. 11-20

Miller, K.G., Browning, J.V., Mountain, G.S., Bassetti, M.A., Monteverde, D., Katz, M.E., Inwood, J., Lofi, J., Proust, J-N., 2013a, Sequence boundaries are impedance contrasts: Core-seismic-log integration of Oligocene-Miocene sequences, New Jersey shallow shelf: *Geosphere*, v. 9, p. 1257-1285

Miller, K.G., Mountain, G.S., Browning, J.V., Katz, M.E., Monteverde, D., Sugarman, P.J., Ando, H., Bassetti, M.A., Bjerrum, C.J., Hodgson, D.M., Hesselbo, S., Karakaya, S., Proust, J-N., Rabineau, M.,

2013b, Testing sequence stratigraphic models by drilling Miocene foresets on the New Jersey Shallow Shelf: *Geosphere*, v. 9, p. 1236-1256

Mitchum, R.M., Vail, P.R., Thompson, S., 1977, Seismic stratigraphy and global changes in sea level, part 2: the depositional sequence as the basic unit for stratigraphic analysis, *in* Payton, C.E., eds., *Seismic Stratigraphy: Applications to Hydrocarbon Exploration: AAPG Memoir*, v. 26, p. 53-62

Monteverde, D.H., Mountain, G.S., Miller, K.G., 2008, Early Miocene sequence development across the New Jersey margin: *Basin Research*, v.20, p. 249-267

Moore, A., Goff, J., McAdoo, B.G., Fritz, H.M., Gusman, A., Kalligeris, N., Kalsum, K., Susanto, A., Suteja, D., Synolakis, C.E., 2011, Sedimentary Deposits from the 17 July 2006 Western Java Tsunami, Indonesia: Use of Grain Size Analyses to Assess Tsunami Flow Depth, Speed, and Traction Carpet Characteristics: *Pure and Applied Geophysics*, v. 168, p. 1951-1961

Mountain, G.S., Proust, J-N., McInroy, D., Cotteril, C., and the Expedition 313 Scientists, 2010, *Proceedings of the Integrated Ocean Drilling Program, Expedition 313: Tokyo, Integrated Ocean Drilling Program Management, Inc.*

Mulder, T., Alexander, J., 2001, The physical character of subaqueous sedimentary density flows and their deposits: *Sedimentology*, v. 48, p. 269-299

Nelson, T.A., 1983, Time and Method Dependent Size distributions of Fine-Grained Sediment: *Sedimentology*, v. 30, p. 249-259

Olariu, C., 2014, Autogenic process change in modern deltas: lessons from the ancient, *in* Martinius, A.W., Ravnås, R., Howell, J.A., Steel, R.J., and Wonham, J.P., eds., *From Depositional Systems to Sedimentary Successions on the Norwegian Continental Margin: International Association of Sedimentologists, Special Publication 46*, p. 149-166

Olariu, C., Steel, R.J., 2009, Influence of point-source sediment-supply on modern shelf-slope morphology: implications for interpretation of ancient shelf margins: *Basin Research*, v. 21, p. 484-501

Patrino, S., Hampson, G.J., Jackson C, A-L., 2015, Quantitative characterisation of deltaic and subaqueous clinoforms: *Earth Science Reviews*, v. 142, p. 79-119

Pellegrini, C., Maselli, V., Gamberi, F., Asioli, A., Bohacs, K.M., Drexler, T.M., Trincardi, F., 2017, How to make a 350-m-thick lowstand systems tract in 17,000 years: The late Pleistocene Po River (Italy) lowstand wedge: *The Geological Society of America Bulletin*, v. 45, p. 327-330

Peng, Y., Steel, R.J., Olariu, C., 2017, Transition from storm wave-dominated outer shelf to gullied upper slope: The mid-Pliocene Orinoco shelf margin, South Trinidad: *Sedimentology*, v. 64, p. 1511-1539

Petter, A.L., Steel, R.J., 2006, Hyperpycnal flow variability and slope organization on an Eocene shelf margin, central basin, Spitsbergen: *American Association of Petroleum Geologists Bulletin*, v. 90, p. 1451-1472

Pirmez, C., Pratson, L.F., Steckler, M.S., 1998, Clinoform development by advection–diffusion of suspended sediment: modelling and comparison to natural systems: *Journal of Geophysical Research*, v. 103, p. 141-157

Plink-Björklund, P., Mellere, D., Steel, R.J., 2001, Turbidite variability and architecture of sand-prone, deep-water slopes: Eocene clinoforms in the central basin, Spitsbergen: *Journal of Sedimentary Research*, v. 71, p. 895-912

Plink-Björklund, P., Steel, R.J., 2004, Initiation of turbidity currents: outcrop evidence for Eocene hyperpycnal flow turbidites: *Sedimentary Geology*, v. 165, p. 29-52

Posamentier, H.W., Allen, G.P., James, D.P., Tesson, M., 1992, Forced regressions in a sequence stratigraphic framework: Concepts, examples, and exploration significance: American Association of Petroleum Geologists Bulletin, v. 76, p. 1687-170

Reineck, H.E., Singh, I.B., 1972, Genesis of laminated sand and graded rhythmites in storm-sand layers of shelf mud: Sedimentology, v. 18, p. 123-128.

Rich, J.L., 1951, Three critical environments of deposition and criteria for recognition of rocks deposited in each of them: Geological Society of America Bulletin, v. 62, p. 1-20

Rossi, V.M., Steel, R.J., 2016, The role of tidal, wave and river currents in the evolution of mixed-energy deltas: example from the Lajas Formation (Argentina): Sedimentology, v. 63, p. 824-864

Roy, P.S., Cowell, P.J., Ferland, M.A., Thom, B.G., 1994, Wave-dominated coasts, *In* Carter, R.W.G., Woodroffe, C.D., eds., Coastal Evolution: Late Quaternary Shoreline Morphodynamics, Cambridge University Press, p. 121

Ryan, M., Helland-Hansen, W., Johannessen, E.P., Steel, R.J., 2009, Erosional vs accretionary shelf margins: the influence of margin type on deepwater sedimentation- an example from the Porcupine Basin, offshore western Ireland, *in*: Henriksen, S., Hampson, G.J., Helland-Hansen, W., Johannessen, E.P., Steel, R.J., Trajectory Analysis in Stratigraphy: Basin Research, v. 21, p. 676-703

Sahu, B.K., 1964, Depositional Mechanisms for the Size Analysis of Clastic Sediments: Journal of Sedimentary Petrology, v. 34, p. 73-83

Sanchez, C.M., Fulthorpe, C.S., Steel, R.J., 2012, Middle Miocene–Pliocene siliciclastic influx across a carbonate shelf and influence of deltaic sedimentation on shelf construction, northern Carnarvon Basin, Northwest Shelf of Australia: Basin Research, v. 24, p. 664-662

Schumacher, B. A., 2002, Methods for the Determination of Total Organic Carbon (TOC) in Soils and Sediments, Ecological Risk Assessment Support Centre, Office of Research and Development, US Environmental Protection Agency, Las Vegas

Southard, J.B., Stanley, D.J., 1976, Shelf-break processes and sedimentation, *in*: Stanley, D.J., Swift, D.J.P., eds., *Marine Sediment Transport and Environmental Management*, Wiley-Interscience, New York, p. 351-377

Steel, R.J., Olsen, T., 2002, Clinoforms, clinoform trajectory and deepwater sands, *In*: Armentrout, J.M. Rosen, N.C., eds., *Sequence Stratigraphic Models for Exploration and Production: Evolving Methodology, Emerging Models and Application Histories*, Publication, GCS-SEPM Special, p. 367-381

Stevenson, C., Jackson C. A.-L., Hodgson, D.M., Hubbard, S.M., Eggenhuisen, J.T., 2015, Deep-water sediment bypass: *Journal of Sedimentary Research*, v. 87, p. 1058-1081

Sydow, J., Roberts, H., 1994, Stratigraphic framework of a Late Pleistocene shelf-edge delta, northeast Gulf of Mexico: *American Association of Petroleum Geologists Bulletin*, v. 78, p. 1276-1312

Ta, T.K.O., Nguyen, V.L., Tateishi, M., Kobayashi, I., Saito, Y., Nakamura, T., 2002, Sediment facies and Late Holocene progradation of the Mekong River Delta in Bentre Province, southern Vietnam: an example of evolution from a tide-dominated to a tide- and wave-dominated delta: *Sedimentary Geology*, v. 152, p. 313-325

Udden, J.A., 1914, Mechanical composition of clastic sediments: *Bulletin of the Geological Society of America*, v. 25, p. 655-744

Uroza, C.A., Steel, R.J., 2008, A highstand shelf-margin delta system from the Eocene of West Spitsbergen, Norway: *Journal of Sedimentary Geology*, v. 203, p 229-245

Vaasma, T., 2008, Grain-size analysis of lacustrine sediments: a comparison of pre-treatment methods: *Estonian Journal of Ecology*, v. 57, p. 231-243

Vail, P.R., Mitchum, R.M. Jr., Thompson, S., 1977, Seismic stratigraphy and global changes of sea level, part 4, global cycles of relative changes of sea level, *in* Payton, C.E., ed., *Seismic stratigraphy*,

application to hydrocarbon exploration: American Association of Petroleum Geologists Memoir, v. 26, p. 83-97

Vakarelov, B.K., Ainsworth, R.B., 2013, A hierarchical approach to architectural classification in marginal marine systems—bridging the gap between sedimentology and sequence stratigraphy: American Association of Petroleum Geologists Bulletin, v. 97, p. 1121-1161

Van Wagoner, J.C., Posamentier, H.W., Mitchum, R.M. Jr., Vail, P.R., Sarg, J.F., Loutit, T.S., Hardenbol, J., 1988, An overview of the fundamentals of sequence stratigraphy and key definitions, *in* Wilgus, C.K., Hastings, B.S., Ross, C.A., Posamentier, H., Van Wagoner, J., Kendall, C.G.St.C., eds., Sea Level Changes: An Integrated Approach: SEPM, Special Publication, v. 42, p. 39-45

Van Wagoner, J.C., Mitchum, R.M. Jr., Campion, K.M., Rahmanian, V.D., 1990, Siliciclastic sequence stratigraphy in well logs, cores and outcrops: concepts for high-resolution correlation of time and facies: American Association of Petroleum Geologists, Methods in Exploration Series, v. 7, p. 1-55

Wear, C.M., Stanley, D.J., Boula, J.E., 1974, Shelf break physiography between Wilmington and Norfolk canyons: Journal of Marine Science and Technology, v. 8, p. 37-48

Wentworth CK., 1922, A scale of grade and class terms for clastic sediments: Journal of Geology, v. 30, p. 377-392

Wilson, M.D., Pittman, E.D., 1977, Authigenic Clays in Sandstones: Recognition and Influence on Reservoir Properties and Palaeoenvironmental Analysis: Journal of Sedimentary Petrology, v. 47, p. 3-31

FIGURE CAPTIONS

- 1- Location map of New Jersey sea level transect, modified from Expedition 313 Scientists (2010). Study sites used in this paper (Integrated Ocean Drilling Program [IODP] Expedition 313 Sites M27, M28 and M29) are presented as purple circles. The seismic profiles indicated represent data acquisition from three different cruises as part of the New Jersey sea-level transect (R/V *Erwing* cruise EW9009, R/V *Oceanus* cruise Oc270 and R/V *Cape Hatteras* cruise CH0698; Monteverde *et al.*, 2008; Mountain *et al.*, 2010; Miller *et al.*, 2013a). The seismic line transecting the core sites M27-M29 (Oc270 529) is indicated in blue. This seismic transect is shown in Figure 2.
- 2- Seismic line Oc270 529. Sequence boundaries relevant to this study are highlighted in red. Depositional sequences analysed in this study are highlighted in various colours, where the yellow clinothem is Sequence m5.7, the green clinothem is Sequence m5.45, the blue clinothem is Sequence m5.4 and the orange clinothem is Sequence m5.3. Depositional sequences are named in according to their basal reflector boundary, for example Sequence m5.7 lies on reflector m5.7. All seismic interpretations are from Monteverde *et al.* (2008), Mountain *et al.* (2010) and Browning *et al.* (2013). Position of clinofold rollovers are indicated by the grey circles.
- 3- Representative core photographs of Clinothem sequences m5.7 (a-c), m5.45 (d-f), m5.4 (g-i) and m5.3 (j-l), showing topset, foreset and bottomset deposits. Photographs show: a) gravelly quartz- and glauconite-rich sands; b) gravelly glauconite-rich sands; c) glauconite- and quartz-rich structureless sands; d) convex-up lamination interpreted as hummocky cross-stratification; e) clean fine sands; f) sandy-silts with minor glauconite; g) parallel laminae of sand and silt; h) finely laminated silts; i) structureless fine sands; j) silts containing shell-fragments and organic matter, k) quartz- and glauconite-rich sands and l) glauconite- and quartz-rich structureless sands.
- 4- Average grain size distribution plots for the topset, foreset and bottomset deposits of Sequences m5.7 (4a), m5.45 (4b), m5.4 (4c) and m5.3 (4d). Y and X axes are percentage volume (%) and grain size (mm), respectively. Alongside the numerical grain size classes are

the descriptive grain size classes modified from Udden (1914) and Wentworth (1922). Topset, foreset and bottomset grain size distributions are shown in red, green and dark brown respectively.

- 5- Box and whisker plots for Sequence m5.7 showing a) grain size, b) sorting, c) sphericity and d) roundness for Cores M27, M28 and M29. The horizontal red line indicates the median; the mean is shown as a green circle; the boundaries of the box indicate the 25th and 75th percentile; whiskers are minimum and maximum values and outliers are shown as blue circles. $n = x$ represents sample size and is shown in Figure 5a.
- 6- Grain-size cumulative frequency plot for topset (5a), foreset (5b) and bottomset (5c) deposits of Sequence m5.7. Y and X axes are depth in meters composite depth (mcd) and grain size by percentage volume (%), respectively. Pie charts showing average grain-size composition by percentage volume for topset (4d), foreset (4e) and bottomset (4f) deposits. The percentage volume for each grain size is also indicated numerically. The number of samples is indicated by $n = x$.
- 7- Box and whisker plots for Sequence m5.45 showing a) grain size, b) sorting, c) sphericity and d) roundness for Cores M27, M28 and M29. The horizontal red line indicates the median; the mean is shown as a green circle; the boundaries of the box indicate the 25th and 75th percentile; whiskers are minimum and maximum values and outliers are shown as blue circles. $n = x$ represents sample size and is shown in Figure 7a.
- 8- Grain size cumulative frequency plot for topset (5a), foreset (5b) and bottomset (5c) deposits of Sequence m5.45. Y and X axes are depth in meters composite depth (mcd) and grain size by percentage volume (%), respectively. Pie charts showing average grain-size composition by percentage volume for topset (4d), foreset (4e) and bottomset (4f) deposits. The percentage volume for each grain size is also indicated numerically. The number of samples is indicated by $n = x$.
- 9- Box and whisker plots for Sequence m5.4 showing a) grain size, b) sorting, c) sphericity and d) roundness for Cores M27, M28 and M29 The horizontal red line indicates the median; the

mean is shown as a green circle; the boundaries of the box indicate the 25th and 75th percentile; whiskers are minimum and maximum values and outliers are shown as blue circles. $n = x$ represents sample size and is shown in Figure 9a.

- 10- Grain size cumulative frequency plot for topset (5a), foreset (5b) and bottomset (5c) deposits of Sequence m5.4. Y and X axes are depth in meters composite depth (mcd) and grain size by percentage volume (%), respectively. Pie charts showing average grain-size composition by percentage volume for topset (4d), foreset (4e) and bottomset (4f) deposits. The percentage volume for each grain size is also indicated numerically. The number of samples is indicated by $n=x$.
- 11- Grain size cumulative frequency plot for topset (5a), foreset (5b) and bottomset (5c) deposits of Sequence m5.3. Y and X axes are depth in meters composite depth (mcd) and grain size by percentage volume (%), respectively. Pie charts showing average grain-size composition by percentage volume for topset (4d), foreset (4e) and bottomset (4f) deposits. The percentage volume for each grain size is also indicated numerically. The number of samples is indicated by $n=x$.
- 12- Box and whisker plots for Sequence m5.3 showing a) grain size, b) sorting, c) sphericity and d) roundness for Cores M27, M28 and M29. The horizontal red line indicates the median; the mean is shown as a green circle; the boundaries of the box indicate the 25th and 75th percentile; whiskers are minimum and maximum values and outliers are shown as blue circles. $n = x$ represents sample size and is shown in Figure 12a.
- 13- Average grain size distribution plots comparing the topset, foreset and bottomset deposits of Type A and Type B clinothems. Y and X axes are percentage volume (%) and grain size (mm), respectively. Alongside the numerical grain size classes are the descriptive grain size classes modified from Udden (1914) and Wentworth (1922). Figures 9a, b and c compare the topset, foreset and bottomset deposits of Type A clinothems respectively. Figures 9d, e and f compare the topset, foreset and bottomset deposits of Type B clinothems respectively.

14- Idealised Type A and B Clinohem Sequences and associated downdip grain-character changes. Figure 14a shows an idealised Type A, river-dominated clinohem sequence. The topset illustrates a delta-front containing glauconite-rich perched sands, which feed sandy foreset and bottomset deposits. The topset also illustrates the along-strike variability in the depositional environments of river-dominated clinohems. Figure 14b shows an idealised Type B, wave-dominated clinohem sequence. The topset illustrates a characteristic wave-dominated shoreface. The delta front is dominated by longshore sediment drift, which prevents significant transport of sediment into bottomset deposits. The feeder channel illustrates episodic returns to river-dominated conditions, as observed in Sequence m5.45. Figures 14c-e show: c) Mean grain size, shown in mm, for Type A and B clinohems in Cores M27-M29. d) Mean sorting, shown according to Geometric Folk and Ward (1957) Graphical Measures, for Type A and B clinohem sequences in Cores M27-M29. e) Mean sphericity, shown according to the Krumbein Scale (1941), for Type A and B clinohems in Cores M27-M29. f) Mean roundness, shown according to the Krumbein Scale (1941), for Type A and B clinohems in Cores M27-M29.

FIGURES

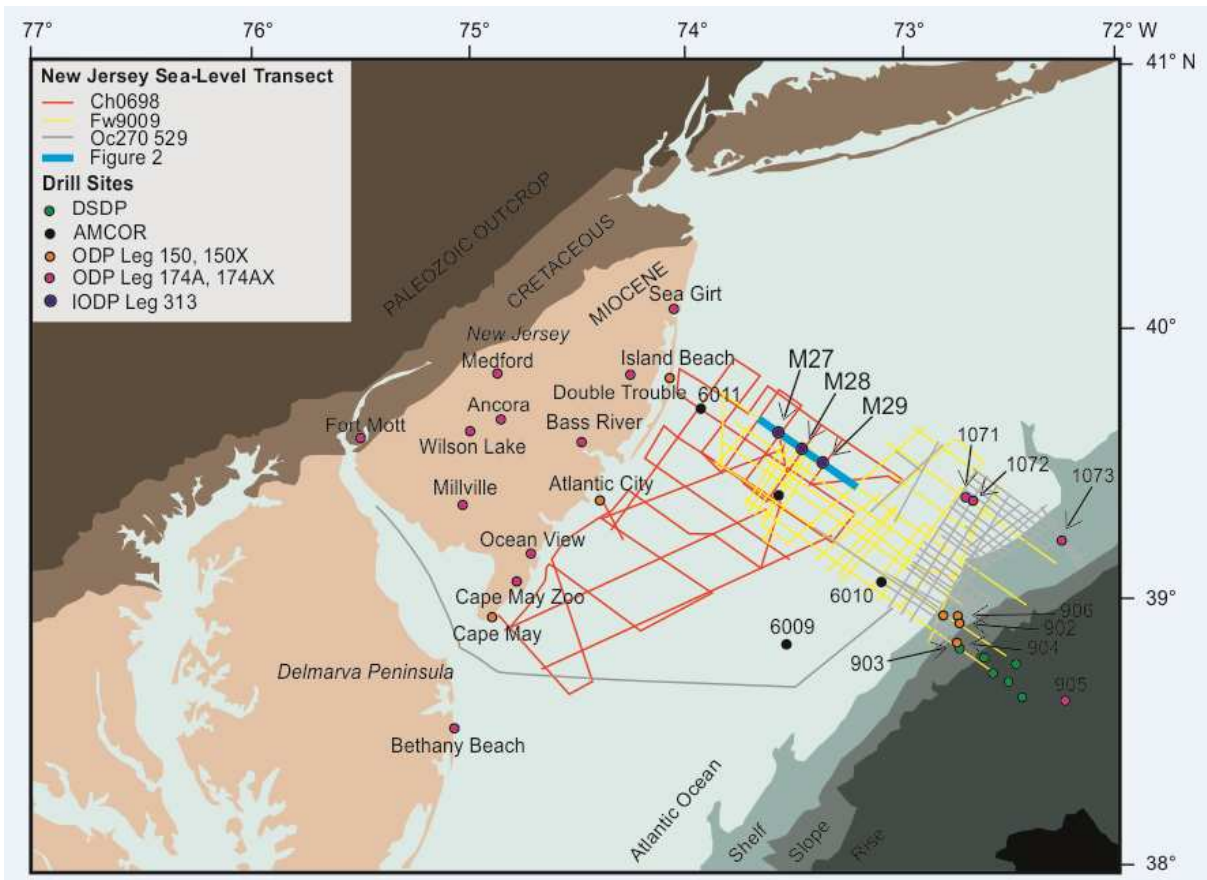


Figure 1

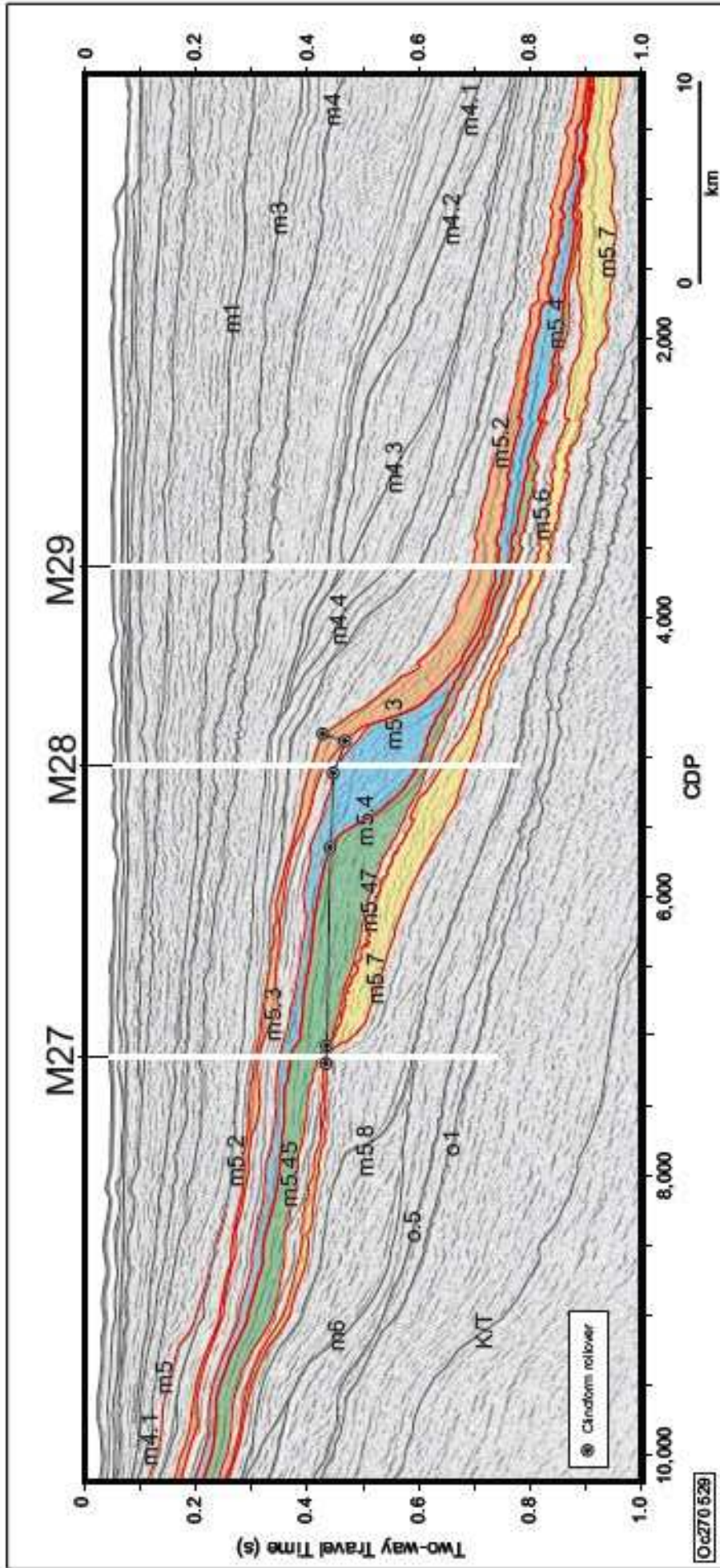


Figure 2


	Topset	Foreset	Bottomset
Sequence m5.7	 <p>Core 313-M27A-116-3</p>	 <p>Core 313-M28A-136-1</p>	 <p>Core 313-M29A-207-3</p>
Sequence m5.45	 <p>Core 313-M27A-107-2</p>	 <p>Core 313-M28A-115-1</p>	 <p>Core 313-M29A-186-2</p>
Sequence m5.4	 <p>Core 313-M27A-96-1</p>	 <p>Core 313-M28A-92-1</p>	 <p>Core 313-M29A-182-2</p>
Sequence m5.3	 <p>Core 313-M27A-85-3</p>	 <p>Core 313-M28A-38-2</p>	 <p>Core 313-M29A-174-1</p>

Figure 3

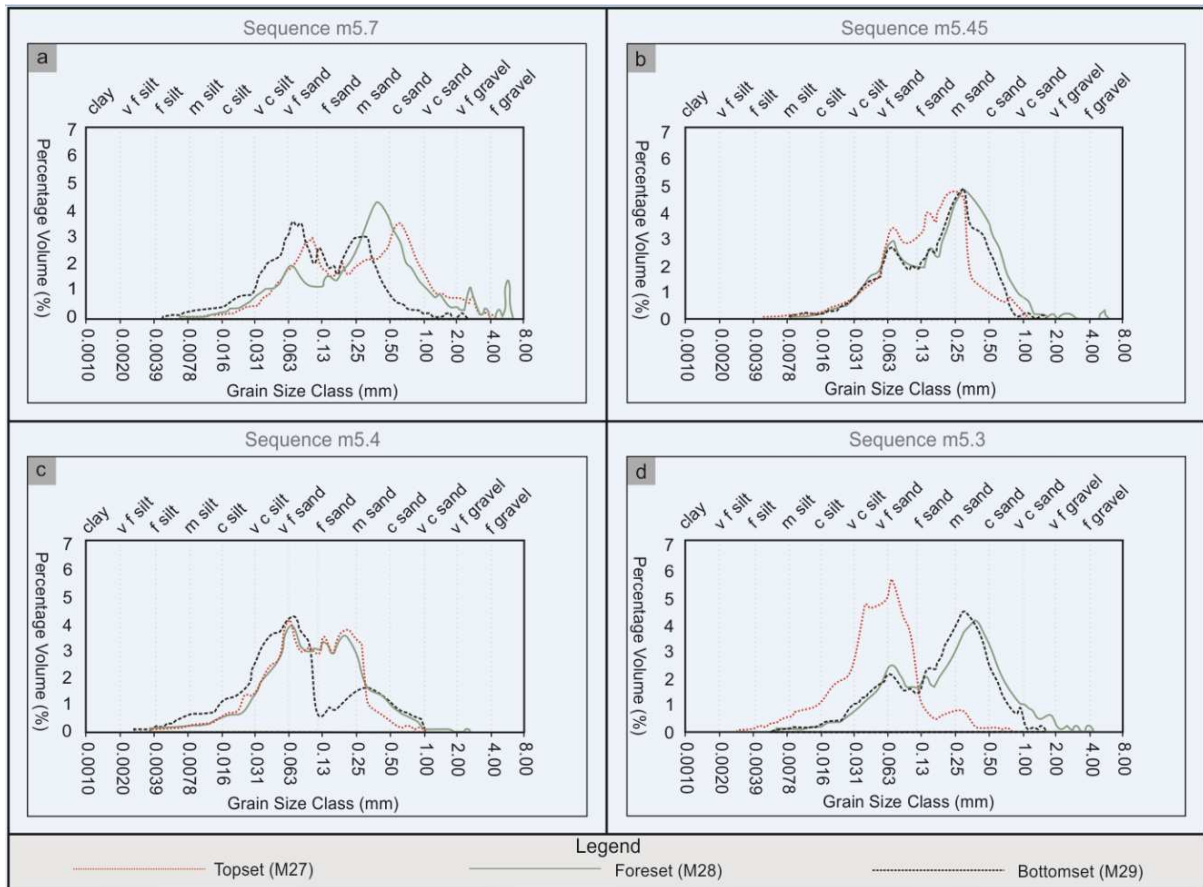


Figure 4

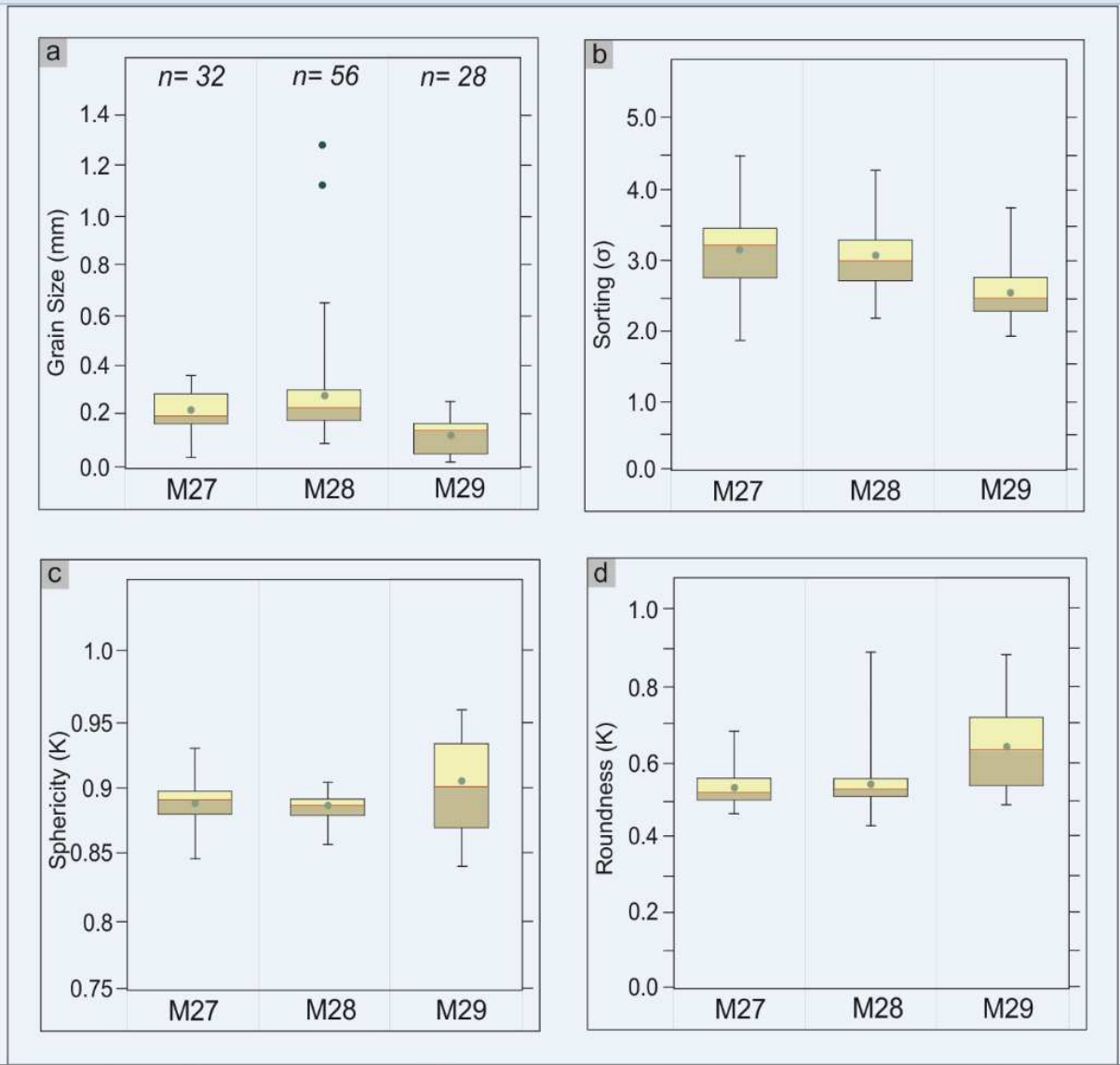


Figure 5

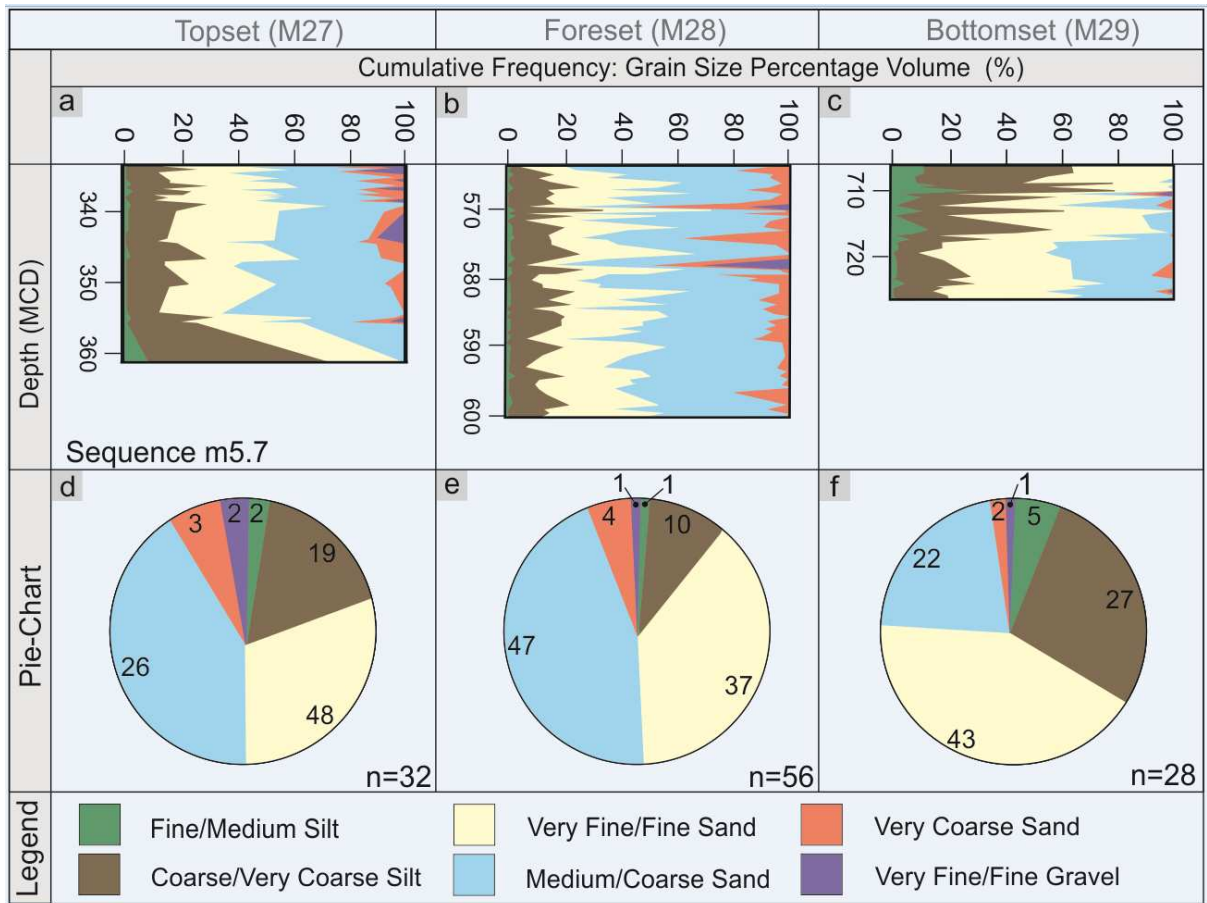


Figure 6

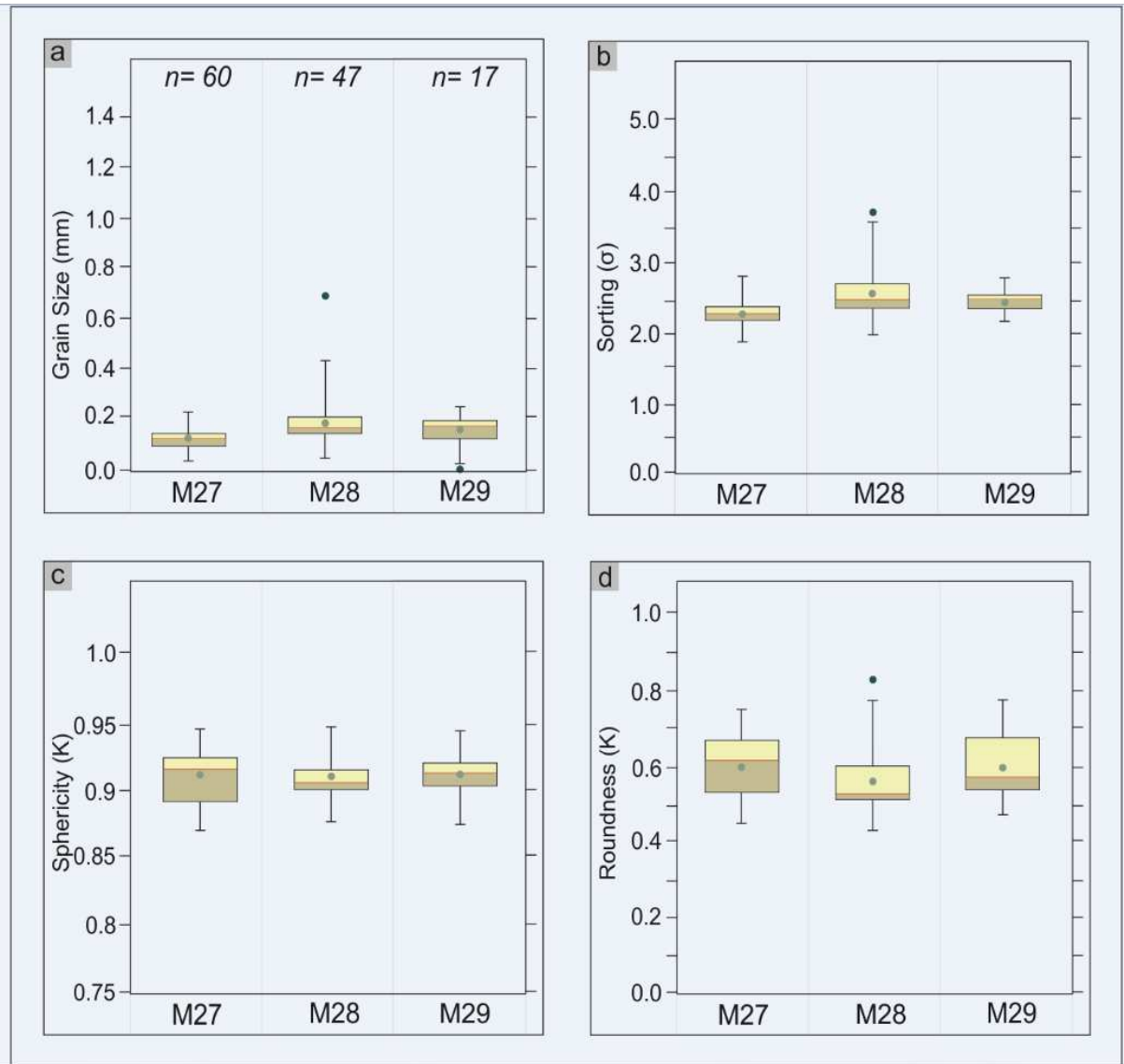


Figure 7

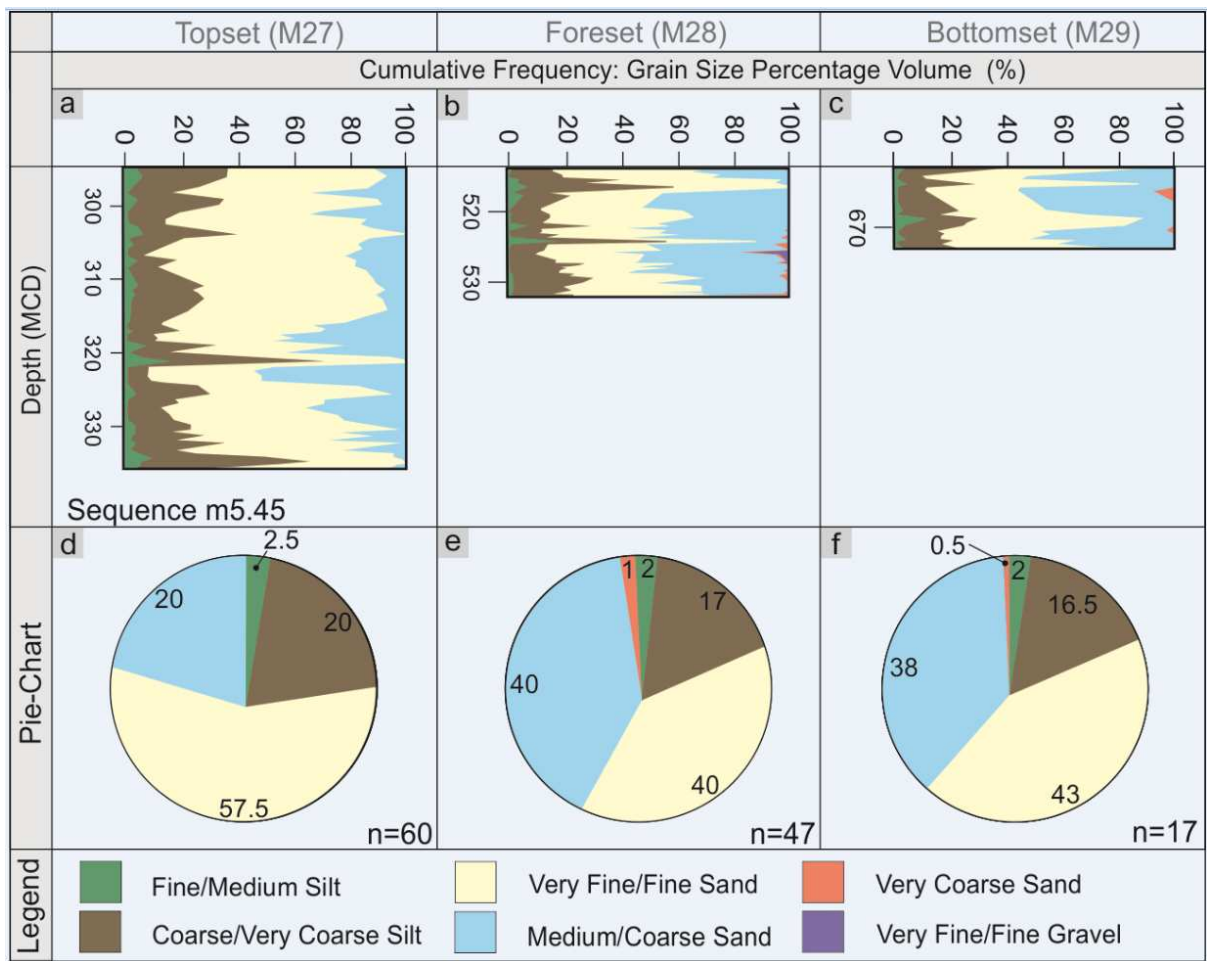


Figure 8

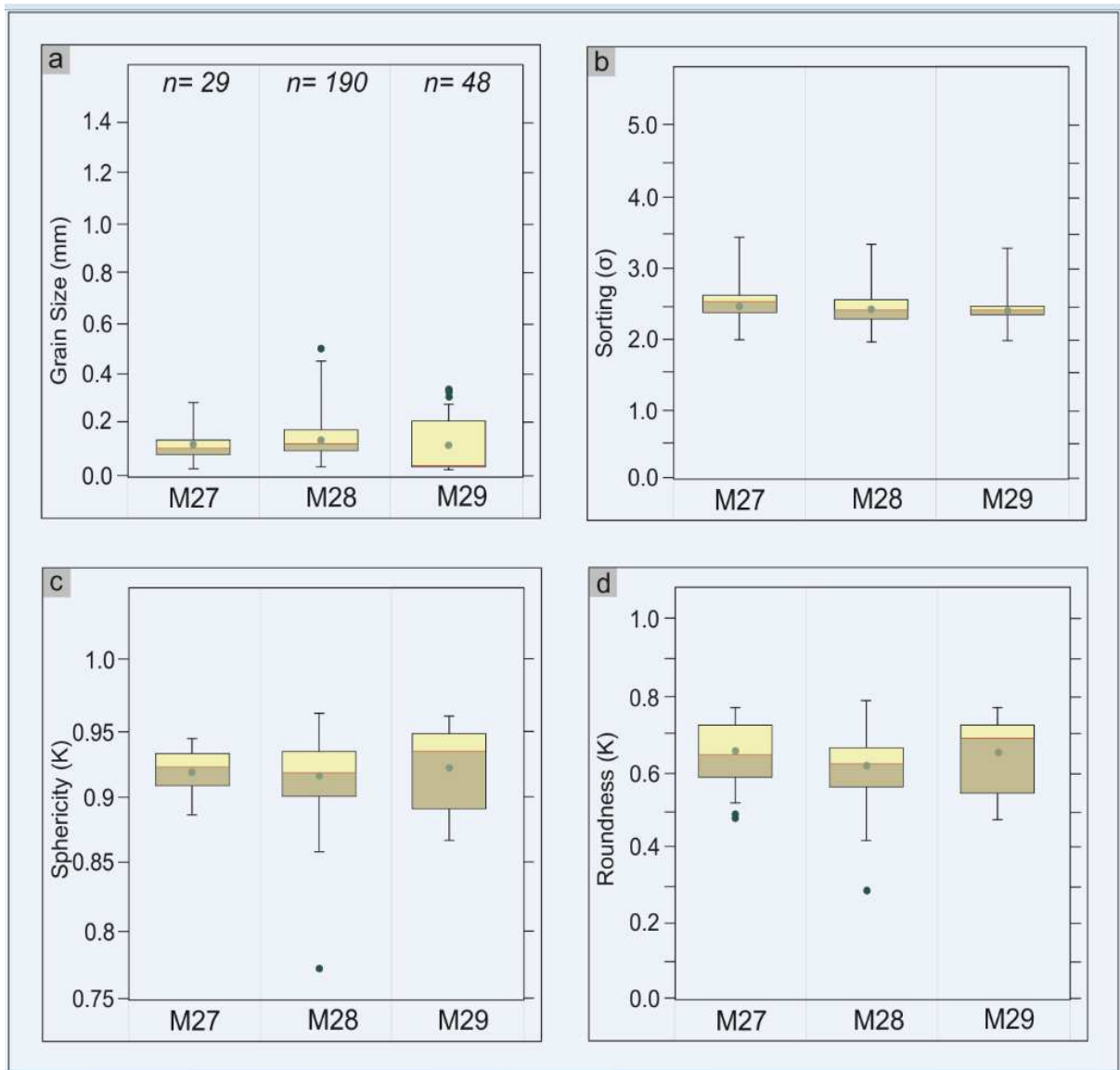


Figure 9

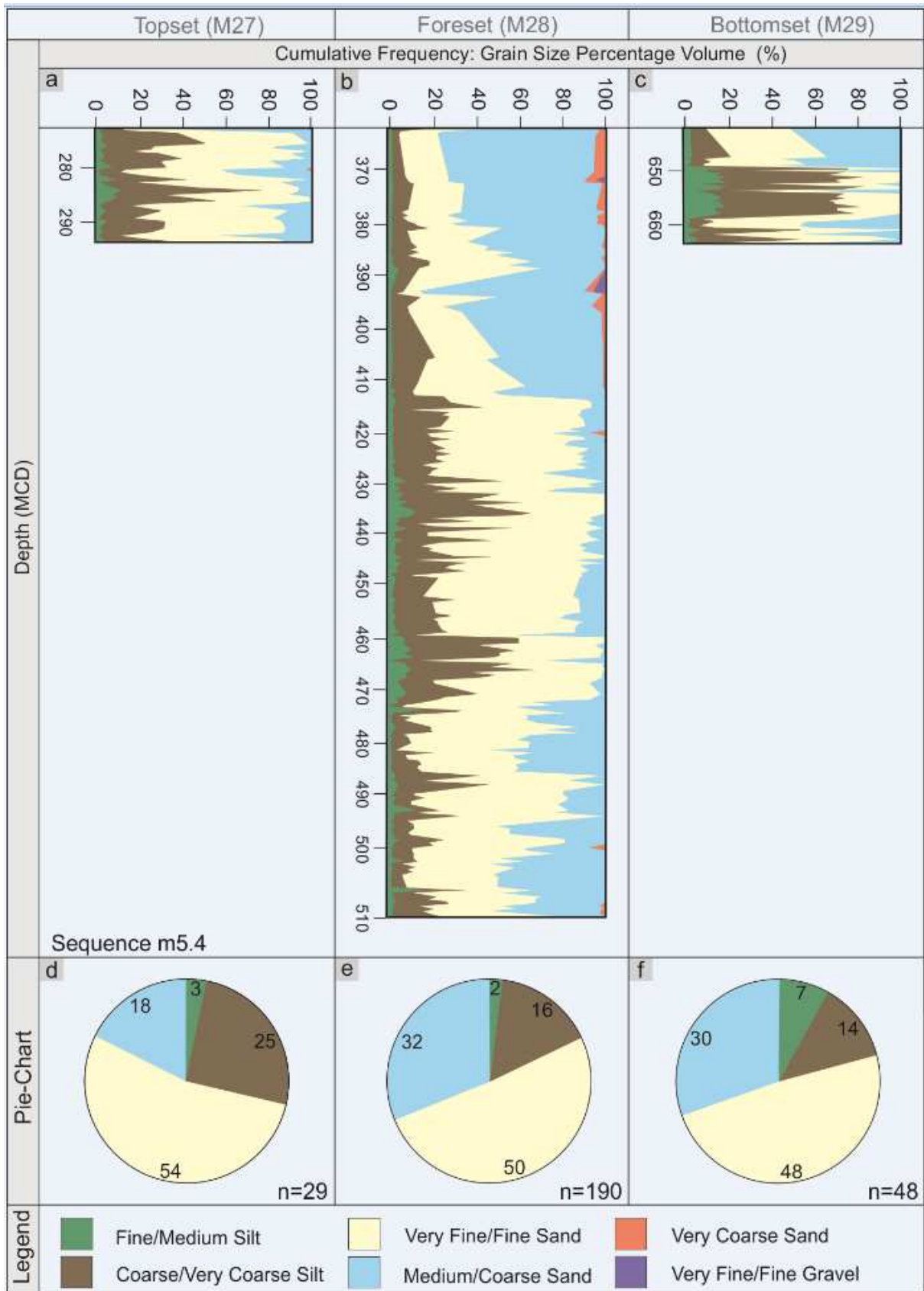


Figure 10

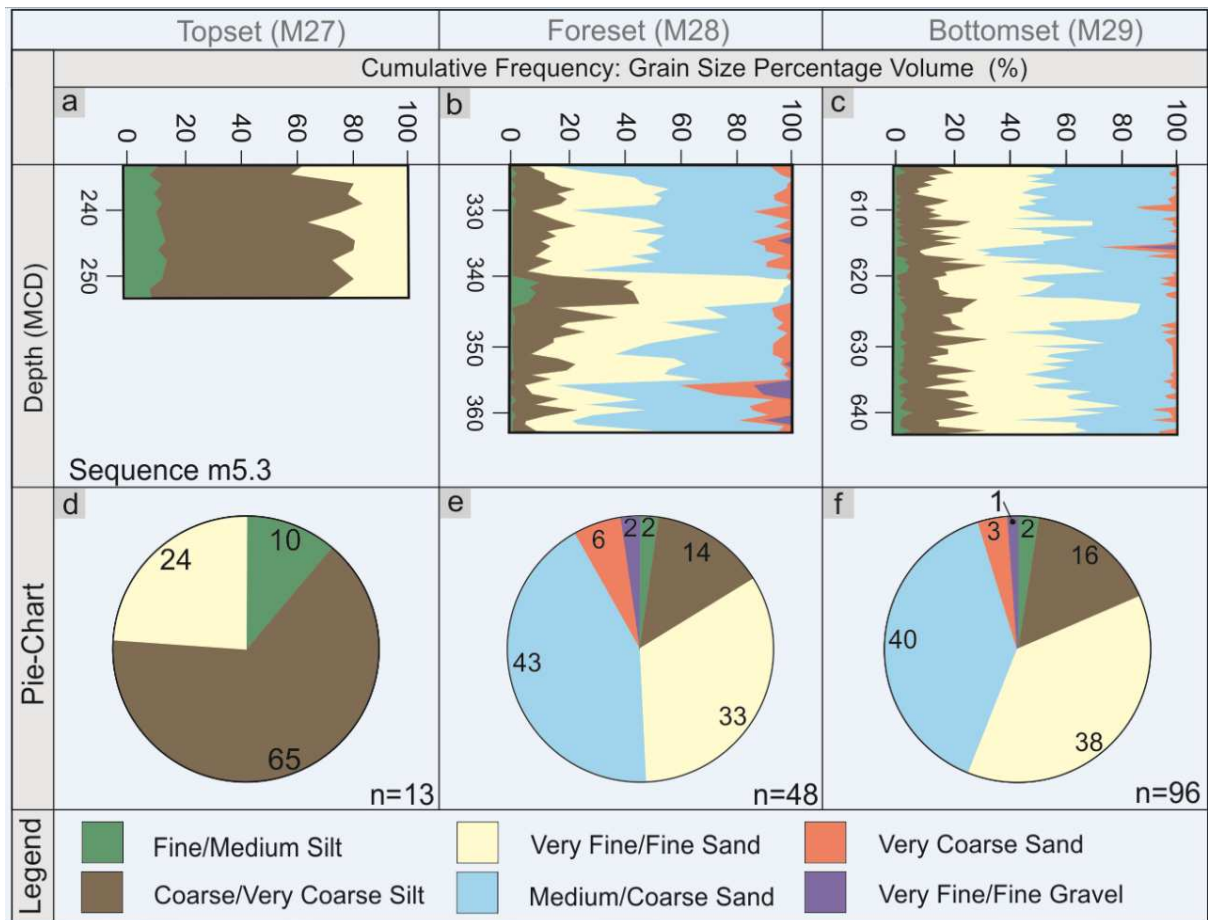


Figure 11

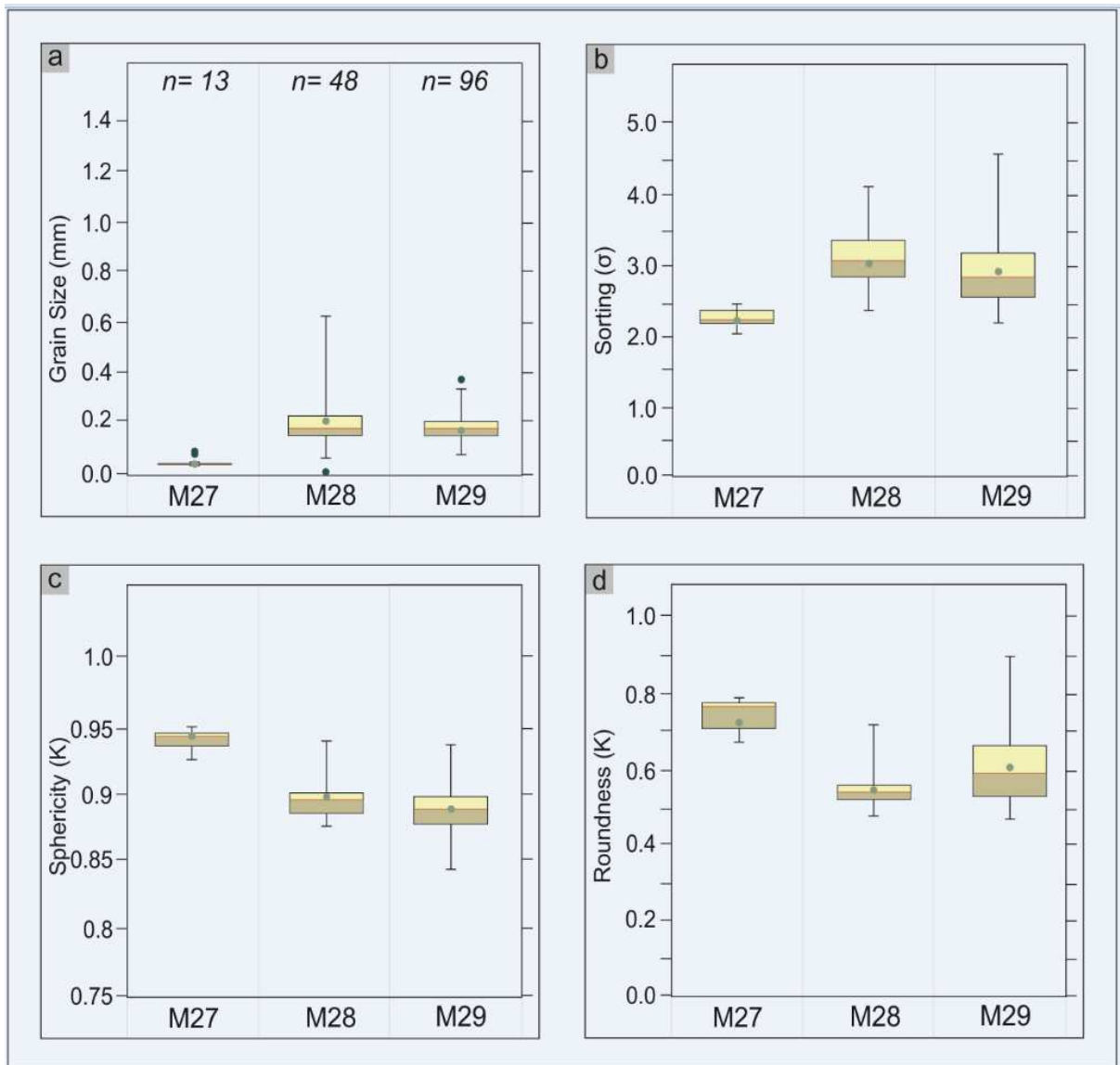


Figure 12

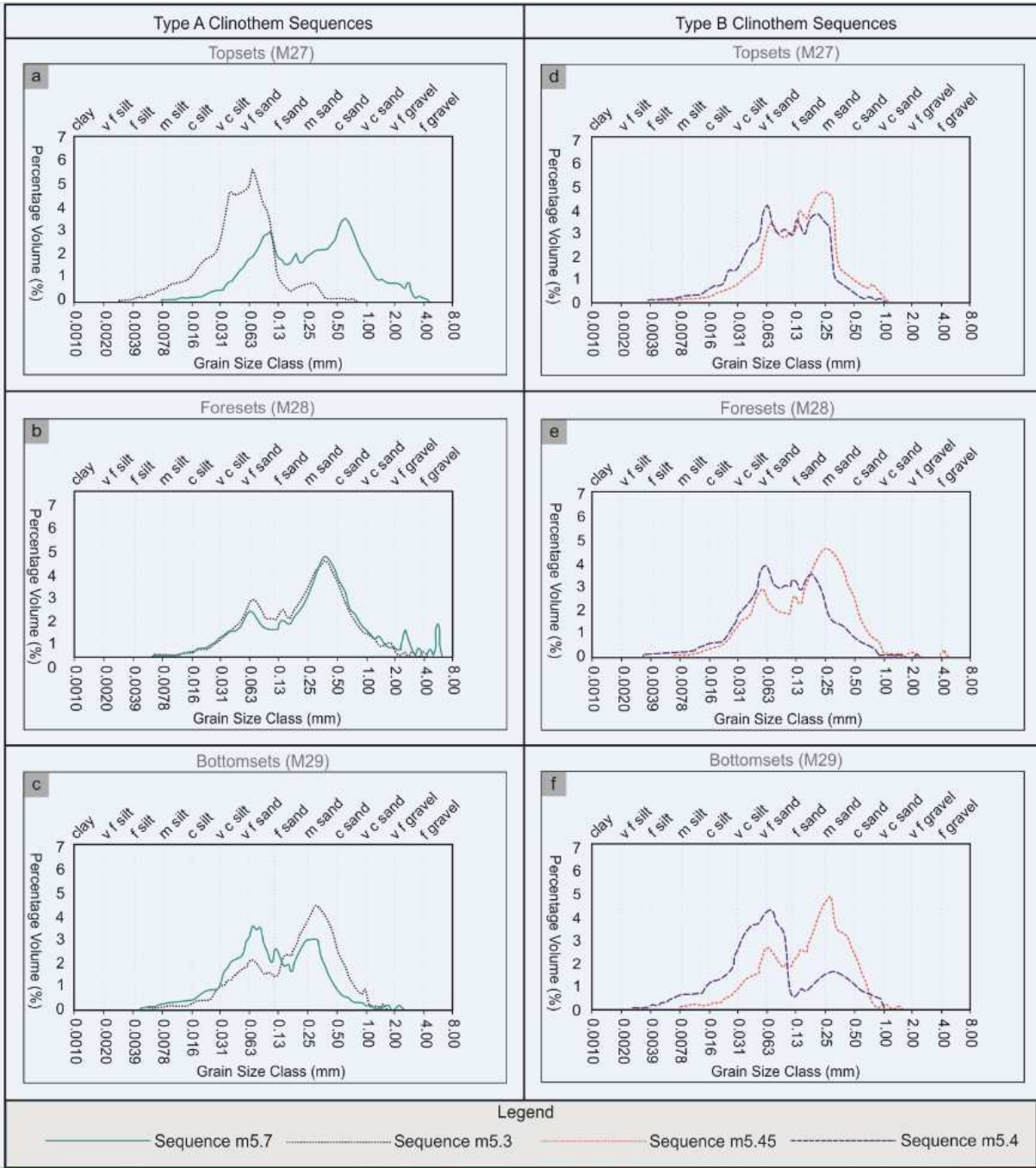


Figure 13

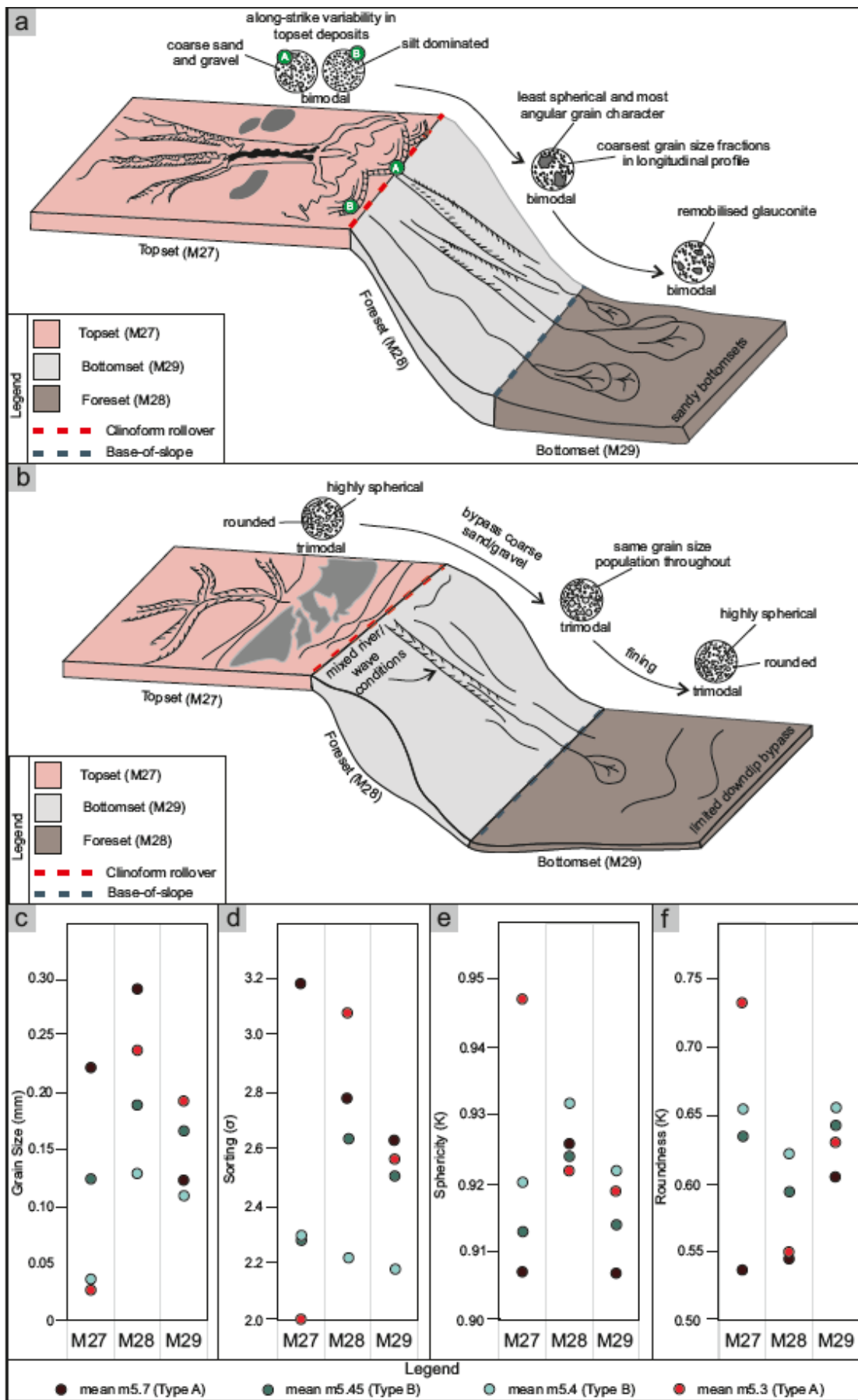


Figure 14